Intrapulse Radar-Embedded Communications Via Multiobjective Optimization

DOMENICO CIUONZO
ANTONIO DE MAIO
Università degli Studi di Napoli Federico II
Napoli, Italy

GOFFREDO FOGLIA
MARCO PIEZZO
ELETTRONICA S.p.A.
Roma, Italy

We deal with the problem of intrapulse radar-embedded communication and propose a novel waveform design procedure based on a multiobjective optimization paradigm. More specifically, under both energy and similarity constraints, we devise signals according to the following criterion: constrained maximization of the signal-to-interference ratio and constrained minimization of a suitable correlation index (which is related to the possibility of waveform interception). This is tantamount to jointly maximizing two competing quadratic forms under two quadratic constraints so that the problem can be formulated in terms of a nonconvex multiobjective optimization. In order to solve it, we resort to the scalarization technique, which reduces the vectorial problem into a scalar one using Pareto weights defining the relative importance of the two objectives. At the analysis stage, we assess the performance of the proposed waveform design scheme in terms of symbol error rate and the so-called intercept metric.

Manuscript received November 3, 2014; revised February 19, 2015; released for publication April 25, 2015.

DOI. No. 10.1109/TAES.2015.140821.

Refereeing of this contribution was handled by S. Blunt.

Part of this paper was presented at the 2015 IEEE International Radar Conference (RadarConf' 15), Arlington, VA, May 2015 (see [1]).

Authors' addresses: D. Ciuonzo, A. De Maio, Università degli Studi di Napoli Federico II, Dipartimento di Ingegneria Elettrica e Tecnologie dell'Informazione, Via Claudio 21, I-80125 Napoli, Italy; G. Foglia, M. Piezzo, ELETTRONICA S.p.A., Via Tiburtina Valeria, Km 13.700, I-00131 Roma, Italy, E-mail: (domenico.ciuonzo@ieee.org).

I. INTRODUCTION

The capability of establishing covert communication has always represented a critical issue for defense-related applications where one among the key aspects is the possibility of hiding sensitive information from hostile interceptors. Over the years, various strategies have been proposed as viable means of masking data transmission; excellent discussions on the topic can be found in [2, 3].

An interesting option consists in directly exploiting a waveform that is already present in the probed environment, such as preexisting communication transmissions [4] or actual radar backscattered interference [5–7]. In this case, a radio frequency (RF) tag/transponder, such as an RF identifier (RFID) [8], is first employed to suitably remodulate the incident radiation and then to embed the devised communication signal in the ambient electromagnetic background, thus providing a natural masking in a dense and cluttered environment. Research in this class of approaches has been quite fertile; in fact, starting from the seminal work of [9] (who introduced the idea of using modulated reflectors for communication), various tag-based radar-embedded (REM) modulation techniques have been proposed. We may cite, for instance, [5, 10, 11], where the radar illumination is modulated on an interpulse basis applying phase-shift sequences over known coherent processing intervals (CPI). However, even though a low probability of intercept (LPI) is ensured (because the signaling is covert by the radar backscatter), the provided data rate is low (on the order of bits-per-CPI). Such a data rate can be acceptable only in very special cases [2] but, unfortunately, in general the aforementioned rate is too low to establish an acceptable communication link. More recently, in [12], an overview discussion on possibilities and challenges for coexistence of radar operations and communication systems was provided. Additionally, a theoretical study on achievable information bounds for radar and communication systems coexistence appeared in [13].

In [2], the authors propose a novel intrapulse REM communication procedure based on the remodulation of the incident radar signaling, through an RF tag/transponder (within the probed environment), into one of the possible K different communication waveforms (acting as information symbols). Three approaches to the waveform design problem have been presented and thoughtfully investigated. The idea is to properly exploit the natural masking provided by the ambient scatter, by devising symbols sharing a certain correlation with the surrounding radar reflections, so as to make very hard the recovery of the information for a hostile eavesdropper, thus ensuring a LPI. Moreover, the transmit sequences are sufficiently separated (ideally orthogonal) with one another in order to minimize mutual interference, thus ensuring a low symbol error rate (SER) or bit error rate, and should be distant enough from the backscatter in order to allow the intended receiver to correctly extricate the useful signal. This is achieved designing communication waveforms that reside

in (or very close to) the passband of the incident radar illumination, temporally (fast-time phase and amplitude) modulating them in order to possess a manageable level of correlation with the radar scattering. Further developments of the proposed approach are also presented in [3], where two notable enhancements consist in the assessment of the benefits of time-reversal for multipath mitigation and a combined two-stage detection/waveform classification scheme for the destination receiver to self-synchronize without the need for prior cueing.

Intuitively, a trade-off exists between the desire of ensuring a low SER and keeping a low profile in the communication. In fact, on the one hand, in order to ensure that the embedded signal is LPI, the power injected by the tag has to be kept adequately below the ambient scattering level and the correlation with the backscatter has to be sufficiently high; on the other hand, in order to guarantee satisfying communication error performance, a certain signal-to-interference ratio (SIR) has to be achieved and a suitable separation from the backscatter interference has to be assured. Therefore, following the hint of [2], in the present paper, we propose an intrapulse REM communication design procedure based on the joint optimization of the two aforementioned (conflicting) objectives; namely, we aim at producing weakly correlated symbols capable of maximizing the SIR and minimizing the probability of intercept. The resulting waveform design problem can be cast into a nonconvex multiobjective optimization. The problem is solved with the help of the so-called scalarization technique, i.e., the original vectorial problem is reduced into a scalar one via the use of Pareto-optimal theory [14–16]. We prove that optimal points of the scalarized problem can be always found exploiting hidden convexity through the use of semidefinite programming and the rank-one decomposition theorems [17, 18]. Then, the proposed signals are chosen as Pareto-optimal points of the previously mentioned multiobjective optimization problem. The proposed approach can be seen as a general framework for REM waveform design and includes, as special instances, the simple (but yet effective) waveform designs provided in [2]. Notice that, in [2], it is shown that satisfactory SER values can be achieved suitably canceling the clutter contribution in the dominant portion of the eigenspectrum. This task is accomplished via a decorrelating filter (DF) because, in that case, the standard matched coherent receiver does not ensure an adequately low communication error rate. Conversely, as it will be shown later, the proposed approach attains interesting SER behaviors even when a matched filter (MF) is employed.

The rest of the paper is organized as follows. In Section II, we introduce the received signal model while in Section III we discuss the figure of merits to optimize. In Section IV, we formulate the waveform design problem and present the algorithm providing Pareto-optimal waveforms. In Section V, we assess the performance of the proposed method also in comparison with the intrapulse REM communication techniques of [2]. Finally, in Section VI, we draw conclusions and outline possible future research tracks; a technical proof is deferred to the Appendix.[1]

II. SYSTEM MODEL

We consider the same model as in [2]. Precisely, let $s(t)$, $t \in [0, T]$, be the complex-baseband (with bandwidth B) of the transmit radar waveform illuminating a given area. By sampling the incident illumination at the Nyquist rate (i.e., B complex samples/second), a tag would obtain a discrete representation of the radar waveform, collected in $N \approx BT$ complex samples. However, at Nyquist rate, the radar waveform fully occupies the unambiguous bandwidth, thus leaving no spectral region where the symbol could be embedded.

Therefore, in order to acquire additional degrees-of-freedom (DOFs), the tag oversamples the incident wave at a rate of MB complex samples/second, with $M > 1$ being the oversampling factor. By doing so, additional spectrum can be exploited so as to earn a new covert region where the communication signal can be embedded. An example is herein given in Fig. 1a, where the amplitude spectrum of $s(t)$ for a real-valued linearly frequency modulated (LFM) signal with one-sided bandwidth 750 kHz and duration $T = 133$ μs is shown. The oversampling factor is set to $M = 2$, so that the useful bandwidth is actually doubled; notice that this operation makes available a new frequency region in the spectral tail of the oversampled sequence. Of course, by properly setting M, it is possible to decide how much additional spectral space (viz. DOFs, cf. Fig. 1b) can be made available at the tag.[2]

Let $\boldsymbol{s} \stackrel{\Delta}{=} [\, s(1)\ s(2)\ \ldots\ s(MN)\,]^T$ be the column vector containing the MN samples. As shown in [2], a discrete

[1] We use boldface for vectors $\boldsymbol{a}$ (lower case), and matrices $\boldsymbol{A}$ (upper case). The nth element of $\boldsymbol{a}$ and the (m, ℓ)th entry of $\boldsymbol{A}$ are denoted by $a(n)$ and $\boldsymbol{A}(m, \ell)$, respectively. The transpose, conjugate, Hermitian, Euclidean norm, real part, and trace operators are denoted by the symbols $(\cdot)^T$, $(\cdot)^*$, $(\cdot)^\dagger$, $\|\cdot\|$, $\Re\{\cdot\}$, and $\mathrm{tr}(\cdot)$, respectively. $\boldsymbol{I}$ and $\boldsymbol{0}$ denote the identity matrix and the matrix with zero entries (when not underlined through a subscript, their size will be easily understood from the context), respectively. $\mathbb{R}^N$, $\mathbb{C}^N$, and $\mathbb{H}^N$ are the sets of N-dimensional vectors of real numbers, the sets of N-dimensional vectors of complex numbers, and $N \times N$ Hermitian matrices, respectively. Given a vector $\boldsymbol{a} \in \mathbb{C}^N$, $\mathrm{diag}(\boldsymbol{a})$ indicates the N-dimensional diagonal matrix whose ith diagonal element is $a(i)$, $i = 1, \ldots, N$. The curled inequality symbol $\succeq$ (and its strict form $\succ$) is used to denote generalized matrix inequality: for any $\boldsymbol{A} \in \mathbb{H}^N$, $\boldsymbol{A} \succeq 0$ (resp., $\boldsymbol{A} \succ \boldsymbol{0}$) means that $\boldsymbol{A}$ is a positive-semidefinite (resp., positive-definite) matrix. $\mathcal{R}(\boldsymbol{X})$ denotes the range space of the matrix $\boldsymbol{X}$. For any $x \in \mathbb{C}$, $|x|$ represents its modulus. The letter j denotes the imaginary unit (i.e., $j = \sqrt{-1}$). $\mathbb{E}[\cdot]$ and $\mathrm{var}[\cdot]$ denote the statistical expectation and variance, respectively. Furthermore, $\mathcal{CN}(\boldsymbol{0}, \boldsymbol{R})$ denotes a complex-valued multivariate Gaussian pdf with zero mean vector and covariance $\boldsymbol{R}$. Finally, for any optimization problem $\mathcal{P}$, we denote with $v(\mathcal{P})$ its optimal value.

[2] Clearly, the oversampling factor M cannot be increased indefinitely because constraints on both electromagnetic compatibility and simplicity in tag/intended receiver hardware design have to be met.

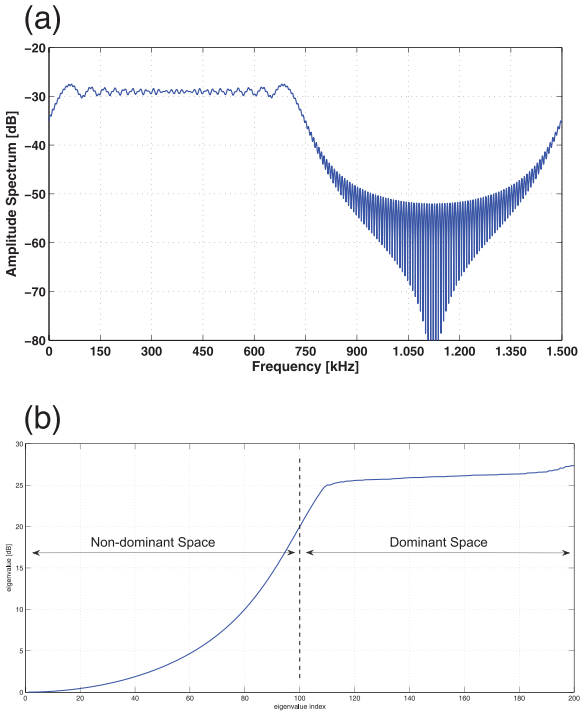

Fig. 1. Complex baseband for LFM signal with $B = 750$ kHz, $T = 133$ μs, $N = 100$, $M = 2$. (a) Amplitude spectrum, (b) sorted eigenvalues of $\boldsymbol{S}\boldsymbol{S}^{\dagger}$.

representation of the radar backscattering model involves the convolution of the discretized sequence $\boldsymbol{s}$ with the discretized version of the aggregate ambient scattering, which can be alternatively expressed in terms of the following matrix multiplication:

$$\boldsymbol{S}\boldsymbol{x} = \begin{bmatrix} s(MN) & s(MN-1) & \dots & s(1) & 0 & \dots & 0 \\ 0 & s(MN) & \dots & s(2) & s(1) & \dots & 0 \\ \vdots & \vdots & \ddots & \vdots & \ddots & \vdots & \vdots \\ 0 & 0 & \dots & s(MN) & s(MN-1) & \dots & s(1) \end{bmatrix} \boldsymbol{x}, \tag{1}$$

where $\boldsymbol{x} \in \mathbb{C}^{(2MN-1)\times 1}$ is the vector containing the range samples of the aggregate ambient radar scattering, and $\boldsymbol{S} \in \mathbb{C}^{MN\times(2MN-1)}$ is the matrix accounting for the shifted versions of the illuminating radar waveform. Also, let $\boldsymbol{c}_k$, $k = 1, \dots, K$, be the kth devised embedded symbol. Therefore, the discretized signal (when kth waveform is transmitted) at the (intentional and/or unintentional) receiver can be expressed, after perfect timing synchronization, as the following $MN \times 1$ vector[3]:

$$\boldsymbol{y}_{rk} = \alpha \boldsymbol{c}_k + \beta \boldsymbol{S}\boldsymbol{x} + \boldsymbol{n}\,, \tag{2}$$

where $\alpha \in \mathbb{C}$ is the (unknown) echo amplitude (accounting for the transmit amplitude and channels propagation effects), $\beta \in \mathbb{R}^{+}$ subsumes the strength of the interference sources, and $\boldsymbol{n} \in \mathbb{C}^{MN\times 1}$ is the vector of the noise samples.

[3] Hereinafter, we will use the notation $\boldsymbol{y}_r$ when the actual symbol transmitted is not known at the receiver.

Without loss of generality, with reference to $\boldsymbol{x}$ and $\boldsymbol{n}$, we draw out both vectors from independent white Gaussian distributions, i.e., $\boldsymbol{x} \sim \mathcal{CN}(\boldsymbol{0}, \frac{1}{MN}\boldsymbol{I})$ and $\boldsymbol{n} \sim \mathcal{CN}(\boldsymbol{0}, \frac{1}{MN}\boldsymbol{I})$, in order to account for the average power of the embedded communication signal and that of the autointerference directly in α and β, respectively. Indeed, by doing so, the input signal-to-noise ratio (SNR) and SIR when the kth waveform is transmitted are given by:

$$\begin{aligned} \mathrm{SNR}_k &\triangleq \mathbb{E}\left[\|\alpha \boldsymbol{c}_k\|^2\right] / \mathbb{E}\left[\|\boldsymbol{n}\|^2\right] = |\alpha|^2 \|\boldsymbol{c}_k\|^2; \\ \mathrm{SIR}_k &\triangleq \mathbb{E}\left[\|\alpha \boldsymbol{c}_k\|^2\right] / \mathbb{E}\left[\|\beta \boldsymbol{S}\boldsymbol{x}\|^2\right] = \frac{|\alpha|^2 \|\boldsymbol{c}_k\|^2}{\beta^2 \|\boldsymbol{s}\|^2}. \end{aligned} \tag{3}$$

III. PERFORMANCE MEASURES

In this section, we focus on the key performance measures to optimize or control in the selection of the modulating code.

A. Output SIR

As already stated, it is necessary, for demodulation purposes at the intended receiver, to have the exact knowledge of the K possible communication symbols transmitted by the tag. Thus, a set of properly designed K filters, say $\boldsymbol{w}_k$, $k = 1, \dots, K$, are assumed at receiver side. Given the signal model (2), the normalized (output) SIR for the kth REM communication waveform is:

$$\mathrm{SIR}_{o,k} \triangleq \frac{1}{MN} \frac{\mathbb{E}\left[|\boldsymbol{w}_k^{\dagger}\boldsymbol{c}_k|^2\right]}{\mathbb{E}\left[|\boldsymbol{w}_k^{\dagger}\boldsymbol{S}\boldsymbol{x}|^2\right]} = \frac{|\boldsymbol{w}_k^{\dagger}\boldsymbol{c}_k|^2}{\boldsymbol{w}_k^{\dagger}(\boldsymbol{S}\boldsymbol{S}^{\dagger})\boldsymbol{w}_k}. \tag{4}$$

It is well-known [19] that the filter maximizing (4) has the form $\boldsymbol{w}_k^{\star} = (\boldsymbol{S}\boldsymbol{S}^{\dagger})^{-1}\boldsymbol{c}_k$, which, after substitution, leads to the optimized kth normalized SIR:

$$\mathrm{SIR}_{o,k}^{\star} = \boldsymbol{c}_k^{\dagger}(\boldsymbol{S}\boldsymbol{S}^{\dagger})^{-1}\boldsymbol{c}_k. \tag{5}$$

The latter metric will be used as a performance measure to achieve low values of SER.

B. Orthogonal Projection

Using model (1), we can obtain a suited orthogonal basis for the waveforms design, computing the eigendecomposition of the correlation matrix of $\boldsymbol{S}$, i.e.,

$$\boldsymbol{S}\boldsymbol{S}^{\dagger} = \boldsymbol{V}\boldsymbol{\Lambda}\boldsymbol{V}^{\dagger}, \tag{6}$$

where $\boldsymbol{\Lambda} = \mathrm{diag}([\,\lambda_1\ \lambda_2\ \dots\ \lambda_{MN}\,]^T)$ is the diagonal matrix of the eigenvalues of $\boldsymbol{S}\boldsymbol{S}^{\dagger}$ (sorted in increasing magnitude, i.e., $\lambda_i \le \lambda_{i+1}$), whereas $\boldsymbol{V} = [\boldsymbol{v}_1\ \boldsymbol{v}_1\ \dots\ \boldsymbol{v}_{MN}]$ contains the corresponding MN eigenvectors. Those belonging to the

nondominant space possess the least correlation with the ambient scatter; thus, they can be exploited to design our communication symbols, so as to lower the SER, at the price of a higher probability of intercept because the communication symbols are not sufficiently covered. Following the so-called dominant projection (DP) approach of [2], we focus on projecting away the designed waveform $\boldsymbol{c}_k$ from the dominant subspace.

To this end, let us define the following quantities:

1) The eigendecomposition $\boldsymbol{S}_{P,k-1}\boldsymbol{S}_{P,k-1}^{\dagger} = \boldsymbol{V}_{P,k-1}\boldsymbol{\Lambda}_{P,k-1}\boldsymbol{V}_{P,k-1}^{\dagger}$, where $\boldsymbol{S}_{P,k-1} \triangleq [\, \boldsymbol{S}\ \boldsymbol{c}_1 \cdots \boldsymbol{c}_{k-1}\,] \in \mathbb{C}^{MN\times(2MN+k-2)}$, $k = 1, \ldots, K$, is the matrix obtained comprising $\boldsymbol{S}$ with the first $(k-1)$th communication waveforms, with the eigenvalues sorted in increasing magnitude (when $k = 1$, $\boldsymbol{S}_{P,0} = \boldsymbol{S}$, $\boldsymbol{V}_{P,0} = \boldsymbol{V}$, and $\boldsymbol{\Lambda}_{P,0} = \boldsymbol{\Lambda}$ hold).

2) The specific index L of the eigenvectors belonging to the nondominant space but close enough to the dominant eigenspectrum. Indeed, L should not be chosen very large because this would imply projection of part of the communication waveforms energy into the dominant space, thus leading to performance loss in terms of SER (and possibly interference to the radar receiver). On the other hand, L should not be taken very small because this would cause a reduction in the DOFs available for the waveform design. For instance, a typical choice of L would be $L = (M-1)\,N$, i.e., considering the relevant energy of the radar waveform confined to highest N eigenvalues.

3) $\boldsymbol{V}_{D,k-1} \triangleq [\, \boldsymbol{v}_{L-(k-1)+1} \cdots \boldsymbol{v}_{MN}\,]$ contains the $(MN-L+k-1)$ eigenvectors comprising the dominant space of $\boldsymbol{V}_{P,k-1}$.

4) $\boldsymbol{P}_{k-1}^{\perp} \triangleq \boldsymbol{V}_{D,k-1}\boldsymbol{V}_{D,k-1}^{\dagger}$ and $\boldsymbol{P}_{k-1} \triangleq (\boldsymbol{I} - \boldsymbol{P}_{k-1}^{\perp})$, $k = 1, \ldots, K$, where $\boldsymbol{P}_{k-1}$ projects any waveform away from the space defined by the $(MN-L+k-1)$ vectors of the dominant space of $\boldsymbol{V}_{P,k-1}$.

Then, we search for waveforms complying with

$$\boldsymbol{P}_{k-1}^{\perp}\boldsymbol{c}_k = \boldsymbol{0}\,, \quad k = 1, \ldots, K. \tag{7}$$

This strategy ensures weak correlation among the devised signals (viz. mutual orthogonality in the ideal case of a sharp decay of the dominant space and equal nondominant space eigenvalues); moreover, due to the projection operation, the dominant space is involved as a whole, which confers to the design procedure an improved robustness with respect to other approaches based on the individual eigenvectors (as pointed out and also shown in [2]). Before proceeding further, we remark that a slightly different procedure (which is also intended to ensure projection away from the dominant space) has been successively proposed in [3]. In this latter case, the design of kth waveform is obtained as follows:

$$\boldsymbol{c}_k = \boldsymbol{P}_0\boldsymbol{s}_k, \quad k = 1, \ldots, K, \tag{8}$$

where the $\boldsymbol{s}_k$s are suitably chosen seeds, i.e., drawn from a pseudorandom sequence [3]. However, in this manuscript, we only consider the first approach, i.e., (7), for the following reason. Indeed, the first approach allows keeping the overall computational complexity of our proposed waveform design under control, and enforcing a simultaneous mutual orthogonality for all the waveforms, constructed according to (8), would lead to a (possibly nonconvex) joint optimization for the entire waveform set, with a corresponding dramatic increase in computational complexity. On the other hand, adoption of the metric in (7) allows for a natural sequential (and with reduced complexity) design of the waveforms $\boldsymbol{c}_k$, as it will be shown hereinafter.

C. Energy Constraint

A critical aspect is represented by the energy radiated from the tag. Indeed, the power injected in the illuminated area has to be properly tuned so as to balance between an acceptable SER and a satisfying LPI. Moreover, another key aspect, from a practical point of view, is the actual energy source of the tag because no battery or power source may actually be present to supply an active transmission (this may be the case of passive or semipassive transponder, where a simple passive reflection occurs). Based on these reasons, we enforce an energy constraint, namely:

$$\|\boldsymbol{c}_k\|^2 = 1\,, \quad k = 1, \ldots, K. \tag{9}$$

D. Similarity Constraint

Aiming at increasing the covertness of the symbols, we enforce a spectral similarity with a prescribed unit-norm pseudorandom sequence (denoted here as $\boldsymbol{d}_{0,k}$) over the frequencies belonging to the spectral tail of the oversampled radar signal (e.g., $\approx$ [750, 1500] kHz in Fig. 1a); thus, the communication signal will appear as a noise-like waveform (with a consequent likely flat spectrum) to a hostile eavesdropper scanning the whole spectrum in search for a transmission, making the exchange of information between the transponder and the intended receiver proceed almost unnoticed. The similarity measure adopted here is $\|\boldsymbol{L}\,\boldsymbol{c}_k - \boldsymbol{L}\,\boldsymbol{d}_{0,k}\|^2$, with $\boldsymbol{L}$ being a known matrix [20]. The structure of $\boldsymbol{L}$ that enforces the desired spectral similarity is detailed hereinafter.

First, let $\widehat{\boldsymbol{W}}^{z} \triangleq [\, \boldsymbol{w}_1^T\ \boldsymbol{w}_2^T \cdots \boldsymbol{w}_{\hat{N}}^T\,]^T$ be the $\hat{N}\times\hat{N}$ (with $\hat{N} > MN$) discrete Fourier transform (DFT) matrix whose $\hat{n}$th row ($\hat{n} \in \{1, \ldots, \hat{N}\}$) corresponds to the discrete frequency $\nu_{\hat{n}} \triangleq \frac{\hat{n}-1}{\hat{N}}$, i.e.,

$$\boldsymbol{w}_{\hat{n}} \triangleq \frac{1}{\sqrt{\hat{N}}}\left[\, 1\ e^{-j2\pi\nu_{\hat{n}}} \cdots e^{-j2\pi\nu_{\hat{n}}(\hat{N}-1)}\,\right]. \tag{10}$$

The aforementioned DFT matrix is applied here to the zero-padded waveforms $\boldsymbol{c}_k^{z} \triangleq [\, \boldsymbol{c}_k^T\ 0 \cdots 0\,]^T \in \mathbb{C}^{\hat{N}\times 1}$ and $\boldsymbol{d}_{0,k}^{z} \triangleq [\, \boldsymbol{d}_{0,k}^T\ 0 \cdots 0\,]^T \in \mathbb{C}^{\hat{N}\times 1}$ to allow a finer spectral shaping; clearly, $(\hat{N} - MN)$ denotes the number of appended zeros. Also, we underline that $\boldsymbol{c}_k^{z} = \overline{\boldsymbol{S}}_F\,\boldsymbol{c}_k$ and $\boldsymbol{d}_{0,k}^{z} = \overline{\boldsymbol{S}}_F\,\boldsymbol{d}_{0,k}$ hold, with $\overline{\boldsymbol{S}}_F \triangleq [\, \boldsymbol{I}\ \boldsymbol{0}\,]^T$ being a $\hat{N}\times MN$ selection matrix.

The similarity constraint is here enforced only on a subset of $F < \hat{N}$ discrete frequencies corresponding to the additional tail skirt of the backscattered radar signal spectrum.[4] This operation is formally expressed via the linear operator $\widehat{\boldsymbol{W}}^s \triangleq (\boldsymbol{S}_F\ \widehat{\boldsymbol{W}}^z)$ applied to the generic zero-padded waveform, where $\boldsymbol{S}_F$ denotes a $F \times \hat{N}$ row-selection matrix, e.g., $\boldsymbol{S}_F \triangleq [\,\boldsymbol{0}\ \boldsymbol{I}\,]$. Therefore, based on $\widehat{\boldsymbol{W}}^s$ definition, we can formulate the similarity constraint as

$$\left\| \widehat{\boldsymbol{W}}^s \boldsymbol{c}_k^z - \widehat{\boldsymbol{W}}^s \boldsymbol{d}_{0,k}^z \right\|^2 \leq \epsilon \quad k = 1, \ldots, K, \tag{11}$$

where $\epsilon \geq 0$ is a tunable similarity parameter. Equation (11) can be also equivalently expressed in terms of the nonpadded waveforms as:

$$\left\| \widehat{\boldsymbol{W}} \boldsymbol{c}_k - \widehat{\boldsymbol{W}} \boldsymbol{d}_{0,k} \right\|^2 \leq \epsilon \quad k = 1, \ldots, K, \tag{12}$$

where $\widehat{\boldsymbol{W}} \triangleq (\boldsymbol{S}_F \widehat{\boldsymbol{W}}^z \overline{\boldsymbol{S}}_F) \in \mathbb{C}^{F \times MN}$ represents the matrix that weights only selected frequencies and nonzero samples. Finally, we show that $\epsilon \in [0, 4)$. Indeed, an upper bound to the left-hand side of (11) is obtained as

$$\begin{aligned} \left\| \widehat{\boldsymbol{W}}^s \boldsymbol{c}_k^z - \widehat{\boldsymbol{W}}^s \boldsymbol{d}_{0,k}^z \right\|^2 &\leq \left(\left\| \widehat{\boldsymbol{W}}^s \boldsymbol{c}_k^z \right\| + \left\| \widehat{\boldsymbol{W}}^s \boldsymbol{d}_{0,k}^z \right\| \right)^2 \\ &< \left(\left\| \boldsymbol{c}_k^z \right\| + \left\| \boldsymbol{d}_{0,k}^z \right\| \right)^2 = 4 \end{aligned} \tag{13}$$

where first nonstrict inequality follows from triangle inequality and second inequality is achieved only when both $\boldsymbol{c}_k^z$ and $\boldsymbol{d}_{0,k}^z$ are aligned in the direction of the maximum (unit) eigenvalues of the matrix $\boldsymbol{\Psi} \triangleq ((\widehat{\boldsymbol{W}}^z)^\dagger (\boldsymbol{S}_F^\dagger \boldsymbol{S}_F) \widehat{\boldsymbol{W}}^z)$. Indeed, the aforementioned matrix has the eigenvalue matrix corresponding to $\boldsymbol{S}_F^\dagger \boldsymbol{S}_F$ (we recall that $\widehat{\boldsymbol{W}}^z$ is a unitary matrix); therefore, there will be F orthogonal directions associated to the unit eigenvalue.

E. LPI Metric

In [2], a simple metric is introduced to ascertain how accurately a (intentional or unintentional) receiver, with some prior knowledge on the radar emission $s(t)$ and the oversampling factor M would be able to extract the symbol embedded within the radar backscatter. The key point is represented by the definition of the projection matrix $\tilde{\boldsymbol{P}}_\ell \triangleq (\boldsymbol{I} - \boldsymbol{V}_\ell \boldsymbol{V}_\ell^\dagger)$ for each $\ell \in \{1, \ldots, MN\}$, where $\boldsymbol{V}_\ell \in \mathbb{C}^{MN \times \ell}$ is the matrix of eigenvectors corresponding to the ℓ largest eigenvalues[5] of $\boldsymbol{S}\boldsymbol{S}^\dagger$; compare with (6). The assumption is that the hostile receiver is capable of projecting the received signal $\boldsymbol{y}_{rk}$ over the ℓth projection matrix $\tilde{\boldsymbol{P}}_\ell$, getting the ℓth projection residue $\boldsymbol{z}_k^\ell \triangleq (\tilde{\boldsymbol{P}}_\ell \boldsymbol{y}_{rk})$. By doing so, it is possible to define the normalized correlation with the nth communication waveform as

$$\eta_{n,k}^\ell \triangleq \frac{|\boldsymbol{c}_n^\dagger \boldsymbol{z}_k^\ell|}{\|\boldsymbol{c}_n\| \left\|\boldsymbol{z}_k^\ell\right\|} \quad \ell = 1, \ldots, MN - 1\,, \tag{14}$$

where $|\boldsymbol{c}_n^\dagger \boldsymbol{z}_k^\ell| = |\alpha \boldsymbol{c}_n^\dagger \tilde{\boldsymbol{P}}_\ell \boldsymbol{c}_k + \beta \boldsymbol{c}_n^\dagger \tilde{\boldsymbol{P}}_\ell \boldsymbol{S}\boldsymbol{x} + \boldsymbol{c}_n^\dagger \tilde{\boldsymbol{P}}_\ell \boldsymbol{n}|$. Though not directly connected with the probability of intercept, (14) still represents a viable tool to figure out how accurately the communication waveform (embedded in the radar backscattering) can be extracted by an eavesdropper. Precisely, when $\eta_{n,k}^\ell$ (for a given projection index ℓ) gets higher values, we may infer that $\boldsymbol{c}_n$ has a higher similarity with the waveform embedded in the received signal. In fact, first of all notice that, by construction, the signal $\boldsymbol{c}_n$ is bounded to possess a partial correlation with the ambient backscatter; however, at the same time, it is designed so as to increase the SIR level at the receiver side, which basically is tantamount to enhancing the useful component with respect to the backscattering disturbance term. Hence, it is fair to expect the correlation level with the residue $\tilde{\boldsymbol{P}}_\ell \boldsymbol{S}\boldsymbol{x}$ (which somehow encompasses the backscatter) to be nonnull but yet sufficiently limited. Similarly, due to the independence of the radar transmission from the white thermal noise, we reasonably guess that the correlation between $\boldsymbol{c}_n$ and the residue $\tilde{\boldsymbol{P}}_\ell \boldsymbol{n}$ is quite small. Therefore, with reference to the proposed design technique, our assumption is that the correlation between the signal $\boldsymbol{c}_n$ and the residue $\tilde{\boldsymbol{P}}_\ell \boldsymbol{c}_k$ has a greater impact, over the actual value of the correlation coefficient $\eta_{n,k}^\ell$, than the other two aforementioned components.[6] Given the orthogonal projection involved in (7), the mutual correlation between $\boldsymbol{c}_n$ and the residue $\tilde{\boldsymbol{P}}_\ell \boldsymbol{c}_k$, for $k \neq n$ and $\ell = 1, \ldots, MN - 1$, is designed to be extremely low. Consequently, we infer the correlation index $\eta_{n,k}^\ell$ to be quite small for $k \neq n$, for all $\ell = 1, \ldots, MN - 1$, at least when $k \neq n$; nevertheless, this supposition may be no longer true when $k = n$. Therefore, in order to lower the correlation index $\eta_{n,n}^\ell$, we aim at minimizing the quadratic form $\boldsymbol{c}_n^\dagger \tilde{\boldsymbol{P}}_\ell \boldsymbol{c}_n$ for all $\ell = 1, \ldots, MN - 1$.

Another useful interpretation of the proposed criterion is given by considering a different intercept metric (IM) proposed in [3], which is based on the detection of the communication process. More specifically, for the following hypothesis testing problem

$$\begin{cases} \mathcal{H}_0: & \boldsymbol{y} = \beta \boldsymbol{S}\boldsymbol{x} + \boldsymbol{n} \\ \mathcal{H}_k: & \boldsymbol{y} = \boldsymbol{y}_{rk} = \alpha \boldsymbol{c}_k + \beta \boldsymbol{S}\boldsymbol{x} + \boldsymbol{n}\,, \end{cases} \tag{15}$$

the authors of [3] define the IM statistic:

$$\varepsilon_\ell \triangleq (\boldsymbol{y}^\dagger\ \tilde{\boldsymbol{P}}_\ell\ \boldsymbol{y}) \tag{16}$$

[4] A reasonable choice for F is given by the approximate number of discrete frequencies not occupied by the radar signal, i.e., $F \approx (\frac{M-1}{M})\hat{N}$.

[5] Notice that, when $\ell = MN$, $\tilde{P}_{MN} = \boldsymbol{0}$; hence, we do not consider this projection index.

[6] Of course, it is not the intention of the authors to claim that this statement holds true for all possible design approaches because it clearly depends on the intrapulse modulation technique adopted. Still, our simulations demonstrate the validity of our intuition, at least with respect to the proposed methodology.

which is then compared to a suitable threshold for implementing a detection test at the nonintended receiver. While it is hard to give a complete statistical characterization of (16), we can give an insight based on a characterization up to the second order. Indeed, it can be shown that the mean values under the different hypotheses are given by:

$$\mathbb{E}\left[\varepsilon_\ell|\mathcal{H}_0\right] = \frac{\beta^2}{MN}\sum_{i=1}^{MN-\ell}\lambda_i + \frac{MN-\ell}{MN}, \tag{17}$$

$$\mathbb{E}\left[\varepsilon_\ell|\mathcal{H}_k\right] = |\alpha|^2 \boldsymbol{c}_k^\dagger\,\tilde{\boldsymbol{P}}_\ell\,\boldsymbol{c}_k + \frac{\beta^2}{MN}\sum_{i=1}^{MN-\ell}\lambda_i + \frac{MN-\ell}{MN}, \tag{18}$$

where λ_i are the (sorted) eigenvalues of $\boldsymbol{\Lambda}$, while the variances are given by:

$$\mathrm{var}\left[\varepsilon_\ell|\mathcal{H}_0\right] = \frac{1}{(MN)^2}\mathrm{tr}\left[\tilde{\boldsymbol{P}}_\ell(\beta^2\boldsymbol{S}\boldsymbol{S}^\dagger+\boldsymbol{I})^2\right], \tag{19}$$

$$\mathrm{var}\left[\varepsilon_\ell|\mathcal{H}_k\right] = \frac{1}{(MN)^2}\mathrm{tr}\left[\tilde{\boldsymbol{P}}_\ell(\beta^2\boldsymbol{S}\boldsymbol{S}^\dagger+\boldsymbol{I})^2\right] + \frac{2|\alpha|^2}{MN}\,\boldsymbol{c}_k^\dagger\,\tilde{\boldsymbol{P}}_\ell\,(\beta^2\boldsymbol{S}\boldsymbol{S}^\dagger+\boldsymbol{I})\,\tilde{\boldsymbol{P}}_\ell\,\boldsymbol{c}_k. \tag{20}$$

Therefore, based on the above results, k normal (or modified) deflection measures [21] can be obtained as:

$$\begin{aligned} D_{0,k} &\triangleq \frac{\{\mathbb{E}\left[\varepsilon_\ell|\mathcal{H}_k\right]-\mathbb{E}\left[\varepsilon_\ell|\mathcal{H}_0\right]\}^2}{\mathrm{var}\left[\varepsilon_\ell|\mathcal{H}_0\right]} \\ D_{1,k} &\triangleq \frac{\{\mathbb{E}\left[\varepsilon_\ell|\mathcal{H}_k\right]-\mathbb{E}\left[\varepsilon_\ell|\mathcal{H}_0\right]\}^2}{\mathrm{var}\left[\varepsilon_\ell|\mathcal{H}_k\right]}, \end{aligned} \tag{21}$$

from which it can be inferred whether transmission of the embedded kth waveform can be discerned or not at the nonintended (eavesdropping) receiver. Deflection measures have a long history [22] and, in specific cases (such as Gauss-Gauss shift-in-mean binary testing), they are directly linked to the statistical power of the test under consideration. Nonetheless, in more complicated models (as ours), their use is somewhat arbitrary, even if the literature has shown their effectiveness in some cases. Indeed, the intuitive rationale is that low deflections correspond to a statistic from which it can be hardly inferred the true hypothesis only from its second-order characterization. Because the explicit expressions are

$$D_{0,k} = \frac{\left(|\alpha|^2\boldsymbol{c}_k^\dagger\,\tilde{\boldsymbol{P}}_\ell\,\boldsymbol{c}_k\right)^2}{\mathrm{var}\left[\varepsilon_\ell|\mathcal{H}_0\right]}, \tag{22}$$

$$D_{1,k} = \frac{\left(|\alpha|^2\boldsymbol{c}_k^\dagger\,\tilde{\boldsymbol{P}}_\ell\,\boldsymbol{c}_k\right)^2}{\mathrm{var}\left[\varepsilon_\ell|\mathcal{H}_0\right] + \frac{2|\alpha|^2}{MN}\,\boldsymbol{c}_k^\dagger\,\tilde{\boldsymbol{P}}_\ell\,(\beta^2\boldsymbol{S}\boldsymbol{S}^\dagger+\boldsymbol{I})\,\tilde{\boldsymbol{P}}_\ell\,\boldsymbol{c}_k}, \tag{23}$$

it is apparent that minimization of $D_{i,k}$s is achieved by keeping $\boldsymbol{c}_k^\dagger\,\tilde{\boldsymbol{P}}_\ell\,\boldsymbol{c}_k$ for each waveform as small as possible. Therefore, the proposed measure can also virtually avoid detection of established communication between the transmitter and the intended receiver.

IV. PROBLEM FORMULATION

The idea pursued in this paper is to sequentially design REM communication waveforms, under the orthogonal projection constraint in (7), that jointly optimize the SER performance (through SIR maximization) and the LPI behavior (via minimization of $\boldsymbol{c}_n^\dagger\tilde{\boldsymbol{P}}_\ell\boldsymbol{c}_n$, $\ell = 1,\ldots MN-1$) with a spectral similarity to a known pseudorandom sequence $\boldsymbol{d}_{0,k}$, and an energy constraint.

Based on these reasons, we formulate our problem in terms of a nonconvex multiobjective (with MN objectives) optimization for kth waveform as [14]

$$\mathcal{P}_1 \triangleq \begin{cases} \max\limits_{\boldsymbol{c}_k} & \left(\boldsymbol{c}_k^\dagger(\boldsymbol{S}\boldsymbol{S}^\dagger)^{-1}\boldsymbol{c}_k;\ -\{\boldsymbol{c}_k^\dagger\,\tilde{\boldsymbol{P}}_\ell\,\boldsymbol{c}_k\}_{\ell=1}^{MN-1}\right) \\ \text{s.t.} & \boldsymbol{P}_{k-1}^\perp\boldsymbol{c}_k = \boldsymbol{0}\,, \qquad \boldsymbol{c}_k^\dagger\boldsymbol{c}_k = 1\,, \\ & \|\widehat{\boldsymbol{W}}\boldsymbol{c}_k - \widehat{\boldsymbol{W}}\boldsymbol{d}_{0,k}\|^2 \le \epsilon\,, \end{cases} \tag{24}$$

for $k = 1,\ldots,K$. The interested reader may refer to [14, pp. 174–184] for an exhaustive introduction to the multiobjective optimization and the scalarization technique, whereas examples of the use of the Pareto-optimization theory for radar applications can be found in [16, 23, 24]. The main aspect is the possibility of getting an optimal solution to the starting vectorial problem from an optimal solution of its scalarized version, once a suitable weight vector $\boldsymbol{\zeta} \succ \boldsymbol{0}$ (i.e., a component-wise positive vector) has been defined. Precisely, let

$$\begin{cases} \min_{\boldsymbol{x}} & \boldsymbol{f}_0(\boldsymbol{x}) \\ \text{s.t.} & f_i(\boldsymbol{x}) \le 0\,, \quad h_j(\boldsymbol{x}) = 0\,, \end{cases} \tag{25}$$

be our multiobjective optimization problem, where $\boldsymbol{x} \in \mathbb{R}^n$ is the optimization variable, $f_i(\boldsymbol{x})$, $i = 1,\ldots,m$, and $h_j(\boldsymbol{x})$, $j = 1,\ldots,p$, are the ith inequality constraint and the jth equality constraint function, respectively, and $\boldsymbol{f}_0(\boldsymbol{x}) : \boldsymbol{x} \in \mathbb{R}^n \to \mathbb{R}^q$ is the vector-valued objective function whose q components $F_1(\boldsymbol{x}),\ldots,F_q(\boldsymbol{x})$ can be interpreted as q different scalar objectives, each of which we would like to minimize. Then, an optimal solution to the vectorial problem (also known as Pareto-optimal point) can be obtained through the following scalar problem

$$\begin{cases} \min_{\boldsymbol{x}} & \boldsymbol{\zeta}^T\boldsymbol{f}_0(\boldsymbol{x}) \\ \text{s.t.} & f_i(\boldsymbol{x}) \le 0\,, \quad h_j(\boldsymbol{x}) = 0\,, \end{cases} \tag{26}$$

where the components of the weight vector $\boldsymbol{\zeta} \triangleq [\zeta_1,\ldots,\zeta_q]^T$ define the mutual weights given to each of the scalar objectives in the optimization procedure. Following these guidelines, $\mathcal{P}_1$ can be thus reduced into the following scalarized form

$$\mathcal{P}_2 \triangleq \begin{cases} \max\limits_{\boldsymbol{c}_k} & \boldsymbol{c}_k^\dagger\left(\frac{\zeta_1}{\lambda_{\max}(\boldsymbol{R})}\boldsymbol{R} - \frac{\zeta_2}{\lambda_{\max}(\tilde{\boldsymbol{P}})}\tilde{\boldsymbol{P}}\right)\boldsymbol{c}_k \\ \text{s.t.} & \boldsymbol{P}_{k-1}^\perp\boldsymbol{c}_k = \boldsymbol{0}\,, \qquad \boldsymbol{c}_k^\dagger\boldsymbol{c}_k = 1\,, \\ & \left\|\widehat{\boldsymbol{W}}\boldsymbol{c}_k - \widehat{\boldsymbol{W}}\boldsymbol{d}_{0,k}\right\|^2 \le \epsilon\,, \end{cases} \tag{27}$$

where $\frac{\zeta_1}{\lambda_{\max}(\boldsymbol{R})} > 0$ and $\frac{\zeta_2}{\lambda_{\max}(\tilde{\boldsymbol{P}})} > 0$ represent the weights, $\boldsymbol{R} \triangleq (\boldsymbol{S}\boldsymbol{S}^\dagger)^{-1}$, and $\tilde{\boldsymbol{P}} \triangleq \sum_{\ell=1}^{MN-1} \tilde{\boldsymbol{P}}_\ell$.

FIRST REMARK It is worth pointing out that, in formulating $\mathcal{P}_2$, we have implicitly assigned the same weight ζ_2 to the last $(MN-1)$ components of the vectorial objective function, namely, $\boldsymbol{\zeta} = [\,\zeta_1\ \zeta_2\ \cdots\ \zeta_2\,]^T \in \mathbb{R}^{MN}$, so that:

$$\begin{aligned}\boldsymbol{\zeta}^T \left[\, \boldsymbol{c}_k^\dagger \boldsymbol{R}\, \boldsymbol{c}_k \ -\boldsymbol{c}_k^\dagger \tilde{\boldsymbol{P}}_1 \boldsymbol{c}_k \ \cdots -\boldsymbol{c}_k^\dagger \tilde{\boldsymbol{P}}_{MN-1} \boldsymbol{c}_k \,\right]^T \\ = \boldsymbol{c}_k^\dagger \left[\zeta_1 \boldsymbol{R} - \zeta_2 \tilde{\boldsymbol{P}}\right] \boldsymbol{c}_k. \end{aligned} \tag{28}$$

We underline that the aforementioned weight set restriction in $\mathcal{P}_2$ is only made for the sake of simplicity and based on the assumption that, in absence of any knowledge on the dominant space, an interceptor should reasonably give equal confidence to all the presumed nondominant spaces $\tilde{\boldsymbol{P}}_\ell$. Indeed, the proposed optimization approach straightforwardly applies also in the general case $\boldsymbol{\zeta} \succ \boldsymbol{0}$. Equally important, we point out that the scalar objectives in (24) are not all concave (actually the normalized SIR is a convex function) and also the unitary energy constraint is not affine. Consequently, the multiobjective optimization under investigation (and consequently the scalarized problem) is not concave. Therefore, we cannot claim that, by varying $\boldsymbol{\zeta} \succ \boldsymbol{0}$ (in our specific case $\zeta_1 > 0$ and $\zeta_2 > 0$), we obtain the entire Pareto trade-off surface for the multiobjective (two-objective) optimization considered. Nonetheless, on the converse, the optimal points found for the scalarized problem under investigation all belong to the Pareto frontier [14] and are thus exploited in this study for the design of waveform $\boldsymbol{c}_k$.

SECOND REMARK We point out that considering all the $\boldsymbol{c}_k^\dagger \tilde{\boldsymbol{P}}_\ell \boldsymbol{c}_k$ in the multiobjective optimization $\mathcal{P}_1$ in (24) (and with the same weight ζ_2 in $\mathcal{P}_2$) is very important in order to ensure a reasonable LPI behavior. In fact, it can be shown that the second term in (28), i.e., $\zeta_2\, \boldsymbol{c}_k^\dagger [\sum_{\ell=1}^{MN-1} \tilde{\boldsymbol{P}}_\ell] \boldsymbol{c}_k$, can be rewritten as

$$\zeta_2 \sum_{t=1}^{MN-1} (MN-t)\, |\boldsymbol{v}_t^\dagger \boldsymbol{c}_k|^2\,, \tag{29}$$

which highlights that the terms $|\boldsymbol{v}_t^\dagger \boldsymbol{c}_k|^2$ in the sum (we underline that each term corresponds to the amount of energy of waveform $\boldsymbol{c}_k$ projected in tth DOF) are not equally weighted and, more specifically, higher confidence (which implies a higher penalization) is given to DOFs associated to smaller λ_ts. Those are the DOFs where waveform masking under the radar backscatter energy is less effective. Finally, we observe that an extremely dominating LPI behavior (viz. ζ_2 is very high) in the overall objective could lead to an excessive allocation of generic waveform energy to the DOFs with higher values λ_t. In such a case, even though the radar backscatter energy may be significant, a peaked (detectable) spectrum could be observed from a simple spectral analysis, thus compromising the LPI behavior with respect to such an approach. In the latter case, enforcing a similarity constraint becomes very important and mitigates this issue.

THIRD REMARK It can be shown that for $\mathcal{P}_1$ the inequality constraint can be safely restricted to be $\epsilon \in [0, 2)$. Indeed the left-hand side of (11) is rewritten as:

$$\begin{aligned}\left\| \widehat{\boldsymbol{W}}^s \boldsymbol{c}_k^z - \widehat{\boldsymbol{W}}^s \boldsymbol{d}_{0,k}^z \right\|^2 = (\boldsymbol{c}_k^z)^\dagger\, \boldsymbol{\Psi}\, \boldsymbol{c}_k^z + (\boldsymbol{d}_{0,k}^z)^\dagger\, \boldsymbol{\Psi}\, \boldsymbol{d}_{0,k}^z \\ -2\Re\left\{ (\boldsymbol{c}_k^z)^\dagger\, \boldsymbol{\Psi}\, \boldsymbol{d}_{0,k}^z \right\} \end{aligned} \tag{30}$$

We then consider a generic feasible solution for $\boldsymbol{c}_k^z = \boldsymbol{a}_k$ of $\mathcal{P}_1$, such that $\|\widehat{\boldsymbol{W}}^s \boldsymbol{a}_k - \widehat{\boldsymbol{W}}^s \boldsymbol{d}_{0,k}^z\|^2 \in [2, 4)$. It is not difficult to show that the vector $\boldsymbol{c}_k^z = -\boldsymbol{a}_k$ has the following properties: 1) it is also a feasible solution for $\mathcal{P}_1$, 2) all the objectives of $\mathcal{P}_1$, attain the same values as in the case of $\boldsymbol{c}_k^z = \boldsymbol{a}_k$, and 3) more importantly, $\|-\widehat{\boldsymbol{W}}^s \boldsymbol{a}_k - \widehat{\boldsymbol{W}}^s \boldsymbol{d}_{0,k}^z\|^2 \in [0, 2)$, which readily follows from a sign change of the real part in (30). Therefore, without loss of generality, we will consider $\epsilon \in [0,2)$ in the rest of the paper.

A waveform $\boldsymbol{c}_k$ optimizes $\mathcal{P}_2$ if and only if it is optimal for the problem $\mathcal{P}_3$, defined as

$$\mathcal{P}_3 \triangleq \begin{cases} \max\limits_{\boldsymbol{c}_k} & \boldsymbol{c}_k^\dagger\, \boldsymbol{T}(\gamma)\, \boldsymbol{c}_k \\ \text{s.t.} & \boldsymbol{P}_{k-1}^\perp\, \boldsymbol{c}_k = \boldsymbol{0}\,, \quad \boldsymbol{c}_k^\dagger \boldsymbol{c}_k = 1\,, \\ & \left\| \widehat{\boldsymbol{W}} \boldsymbol{c}_k - \widehat{\boldsymbol{W}} \boldsymbol{d}_{0,k} \right\|^2 \le \epsilon\,, \end{cases} \tag{31}$$

where $\boldsymbol{T}(\gamma) \triangleq (\boldsymbol{R} - \gamma \tilde{\boldsymbol{P}})$ and $\gamma \triangleq \frac{\zeta_2}{\zeta_1} \frac{\lambda_{\max}(\boldsymbol{R})}{\lambda_{\max}(\tilde{\boldsymbol{P}})} > 0$. The aforementioned claim is evident because the objective functions of $\mathcal{P}_2$ and $\mathcal{P}_3$ are proportional and additionally the feasible sets are the same.

Due to the first constraint, there exists a waveform $\hat{\boldsymbol{c}}_k \in \mathbb{C}^{(L-k+1)\times 1}$ such that $\boldsymbol{c}_k = \boldsymbol{U}_{k-1} \hat{\boldsymbol{c}}_k$, where $\boldsymbol{P}_{k-1} = \boldsymbol{U}_{k-1} \boldsymbol{U}_{k-1}^\dagger$ (i.e., the column matrix of eigenvectors associated to the projector $\boldsymbol{P}_{k-1}$). Hence, $\mathcal{P}_3$ can be reformulated as

$$\begin{cases} \max\limits_{\hat{\boldsymbol{c}}_k} & \hat{\boldsymbol{c}}_k^\dagger \left[\boldsymbol{U}_{k-1}^\dagger \boldsymbol{T}(\gamma) \boldsymbol{U}_{k-1} \right] \hat{\boldsymbol{c}}_k \\ \text{s.t.} & \hat{\boldsymbol{c}}_k^\dagger \hat{\boldsymbol{c}}_k = 1\,, \quad \left\| \widehat{\boldsymbol{W}} \boldsymbol{U}_{k-1} \hat{\boldsymbol{c}}_k - \widehat{\boldsymbol{W}} \boldsymbol{d}_{0,k} \right\|^2 \le \epsilon\,, \end{cases} \tag{32}$$

where we have exploited $\boldsymbol{U}_{k-1}^\dagger \boldsymbol{U}_{k-1} = \boldsymbol{I}$ in expressing concisely the equality constraint. Also, from inspection of (32), it is apparent that the similarity vector should be defined as $\boldsymbol{d}_{0,k} \triangleq \boldsymbol{U}_{k-1} \boldsymbol{d}_k / \|\boldsymbol{U}_{k-1} \boldsymbol{d}_k\|$, with $\boldsymbol{d}_k \in \mathbb{C}^{(L-k+1)\times 1}$ being a pseudorandom vector. Indeed, both the projection and the normalization operations involved in the definition of $\boldsymbol{d}_{0,k}$ are necessary to make feasible the optimization problem because the similarity vector has to be a direction vector belonging to the same

subspace of $\boldsymbol{c}_k$. Problem (32) can be further recast as

$$\mathcal{P}_4 \triangleq \begin{cases} \max\limits_{\hat{\boldsymbol{c}}_k} & \hat{\boldsymbol{c}}_k^\dagger \left[\boldsymbol{U}_{k-1}^\dagger \boldsymbol{T}(\gamma) \boldsymbol{U}_{k-1} \right] \hat{\boldsymbol{c}}_k \\ \text{s.t.} & \hat{\boldsymbol{c}}_k^\dagger \hat{\boldsymbol{c}}_k = 1\,, \\ & \hat{\boldsymbol{c}}_k^\dagger \left[-\boldsymbol{U}_{k-1}^\dagger \widehat{\boldsymbol{W}}^\dagger \widehat{\boldsymbol{W}} \boldsymbol{U}_{k-1} \right] \hat{\boldsymbol{c}}_k \\ & + 2\,\Re \left\{ \left[\boldsymbol{U}_{k-1}^\dagger \widehat{\boldsymbol{W}}^\dagger \widehat{\boldsymbol{W}} \boldsymbol{d}_{0,k} \right]^\dagger \hat{\boldsymbol{c}}_k \right\} \\ & + \left(\epsilon - \boldsymbol{d}_{0,k}^\dagger \widehat{\boldsymbol{W}}^\dagger \widehat{\boldsymbol{W}} \boldsymbol{d}_{0,k} \right) \geq 0. \end{cases} \tag{33}$$

Obviously, if $\hat{\boldsymbol{c}}_k^\star$ is optimal for $\mathcal{P}_4$, then $\boldsymbol{c}_k^\star = \boldsymbol{U}_{k-1} \hat{\boldsymbol{c}}_k^\star$ is optimal for $\mathcal{P}_2$, and vice versa. Hence, without loss of generality, we will focus on $\mathcal{P}_4$ hereinafter. In particular, let us consider the following equivalent (homogeneous) quadratically constrained quadratic programming reformulation:

$$\mathcal{P}_5 \triangleq \begin{cases} \max\limits_{\hat{\boldsymbol{c}}_k, t} & \text{tr}\,(\boldsymbol{Q}_0 \boldsymbol{X}) \\ \text{s.t.} & \text{tr}\,(\boldsymbol{Q}_1 \boldsymbol{X}) \geq 0\,, \quad \text{tr}\,(\boldsymbol{Q}_2 \boldsymbol{X}) = 1\,, \\ & \text{tr}\,(\boldsymbol{Q}_3 \boldsymbol{X}) = 1\,, \\ & \boldsymbol{X} \triangleq \begin{bmatrix} \hat{\boldsymbol{c}}_k \hat{\boldsymbol{c}}_k^\dagger & t^* \hat{\boldsymbol{c}}_k \\ t \hat{\boldsymbol{c}}_k^\dagger & |t|^2 \end{bmatrix}, \end{cases} \tag{34}$$

where the matrices $\boldsymbol{Q}_i$ are defined as follows:

$$\begin{aligned} \boldsymbol{Q}_0 &\triangleq \begin{bmatrix} \boldsymbol{U}_{k-1}^\dagger \boldsymbol{T}(\gamma) \boldsymbol{U}_{k-1} & \boldsymbol{0} \\ \boldsymbol{0} & 0 \end{bmatrix}, \\ \boldsymbol{Q}_1 &\triangleq \begin{bmatrix} -\boldsymbol{U}_{k-1}^\dagger \widehat{\boldsymbol{W}}^\dagger \widehat{\boldsymbol{W}} \boldsymbol{U}_{k-1} & \boldsymbol{U}_{k-1}^\dagger \widehat{\boldsymbol{W}}^\dagger \widehat{\boldsymbol{W}} \boldsymbol{d}_{0,k} \\ \left(\boldsymbol{U}_{k-1}^\dagger \widehat{\boldsymbol{W}}^\dagger \widehat{\boldsymbol{W}} \boldsymbol{d}_{0,k} \right)^\dagger & \epsilon - \boldsymbol{d}_{0,k}^\dagger \widehat{\boldsymbol{W}}^\dagger \widehat{\boldsymbol{W}} \boldsymbol{d}_{0,k} \end{bmatrix}, \\ \boldsymbol{Q}_2 &\triangleq \begin{bmatrix} \boldsymbol{I} & \boldsymbol{0} \\ \boldsymbol{0} & 0 \end{bmatrix}, \qquad \boldsymbol{Q}_3 \triangleq \begin{bmatrix} \boldsymbol{0} & \boldsymbol{0} \\ \boldsymbol{0} & 1 \end{bmatrix}. \end{aligned} \tag{35}$$

Both $\mathcal{P}_4$ and $\mathcal{P}_5$ share the same optimal values (the proof is given in the Appendix), i.e., $v(\mathcal{P}_4) = v(\mathcal{P}_5)$.

Therefore, in order to obtain an optimal solution to $\mathcal{P}_2$, it suffices to focus on $\mathcal{P}_5$. Precisely, we can find an optimal solution $\boldsymbol{X}^*$ to $\mathcal{P}_5$ in two (computationally efficient) steps. The first step involves the solution of the following semidefinite programming problem [25], which is evidently the semidefinite relaxation (SDR) of $\mathcal{P}_5$ obtained from dropping the rank-one constraint on $\boldsymbol{X}$:

$$\mathcal{P}_6 \triangleq \begin{cases} \max\limits_{\boldsymbol{X}} & \text{tr}\,(\boldsymbol{Q}_0 \boldsymbol{X}) \\ \text{s.t.} & \text{tr}\,(\boldsymbol{Q}_1 \boldsymbol{X}) \geq 0\,, \quad \text{tr}\,(\boldsymbol{Q}_2 \boldsymbol{X}) = 1\,, \\ & \text{tr}\,(\boldsymbol{Q}_3 \boldsymbol{X}) = 1\,, \quad \boldsymbol{X} \succeq \boldsymbol{0}. \end{cases} \tag{36}$$

The second step consists in the application of a rank-one matrix decomposition theorem [17, Theorem 2.3] (reported in the following lemma) in order to obtain a vector $\boldsymbol{x}^\star = [\,(z^\star)^T \;\; y^\star\,]^T$ where $\boldsymbol{x}^\star(\boldsymbol{x}^\star)^\dagger$ corresponds to a specific rank-one projection of the optimal solution to $\mathcal{P}_6$, denoted here $\boldsymbol{X}_{\text{sdr}}$. This operation is denoted as $x^\star = \mathcal{D}(\boldsymbol{X}_{\text{sdr}}, \boldsymbol{Q}_0, \boldsymbol{Q}_1, \boldsymbol{Q}_2, \boldsymbol{Q}_3)$ hereinafter. Such a theorem ensures (under certain assumptions, specified in the following) the existence (and gives a constructive procedure to build it) of a rank-one solution $\boldsymbol{x}^\star(\boldsymbol{x}^\star)^\dagger$, obtained starting from $\boldsymbol{X}_{\text{sdr}}$, which attains the same value of the objective and still satisfies all the constraints. Therefore, $\boldsymbol{x}^\star(\boldsymbol{x}^\star)^\dagger = \boldsymbol{X}^\star$ holds. Finally, an optimal solution for $\mathcal{P}_3$ is found as $\hat{\boldsymbol{c}}_k^\star = \boldsymbol{z}^\star / y^\star$, and accordingly an optimal solution to $\mathcal{P}_2$ is obtained as $\boldsymbol{c}_k^\star = \boldsymbol{U}_{k-1} \hat{\boldsymbol{c}}_k^\star$.

LEMMA 1 *Let $\boldsymbol{X} \in \mathbb{H}^N (N \geq 3)$ be a nonzero matrix such that $\boldsymbol{X} \succeq \boldsymbol{0}$ and let $\boldsymbol{A}_i \in \mathbb{H}^{N \times N}$, $i \in \{1, 2, 3, 4\}$, and suppose that $[\,\text{tr}(\boldsymbol{Y}\boldsymbol{A}_1) \cdots \text{tr}(\boldsymbol{Y}\boldsymbol{A}_4)\,]^T \neq \boldsymbol{0}$, for any nonzero matrix $\boldsymbol{Y} \in \mathbb{H}^N$, $\boldsymbol{Y} \succeq \boldsymbol{0}$. Then,*

1) *if rank $(\boldsymbol{X}) \geq 3$, one can find, in polynomial time, a rank-one matrix $\boldsymbol{x}\boldsymbol{x}^\dagger$ such that $\boldsymbol{x}$, whose dependence is underlined as $\boldsymbol{x} = \mathcal{D}_1(\boldsymbol{X}, \boldsymbol{A}_1, \boldsymbol{A}_2, \boldsymbol{A}_3, \boldsymbol{A}_4)$, is in $\mathcal{R}(\boldsymbol{X})$ and*

$$\boldsymbol{x}^\dagger \boldsymbol{A}_i \boldsymbol{x} = \text{tr}\,(\boldsymbol{X}\boldsymbol{A}_i)\,, \quad i \in \{1, 2, 3, 4\}; \tag{37}$$

2) *if rank $(\boldsymbol{X}) = 2$, for any $\boldsymbol{z} \notin \mathcal{R}(\boldsymbol{X})$, one can find a rank-one matrix $\boldsymbol{x}\boldsymbol{x}^\dagger$ such that $\boldsymbol{x}$, whose dependence is underlined as $\boldsymbol{x} = \mathcal{D}_2(\boldsymbol{X}, \boldsymbol{A}_1, \boldsymbol{A}_2, \boldsymbol{A}_3, \boldsymbol{A}_4)$, is in the linear subspace spanned by $\{\boldsymbol{z}\} \cup \mathcal{R}(\boldsymbol{X})$ and*

$$\boldsymbol{x}^\dagger \boldsymbol{A}_i \boldsymbol{x} = \text{tr}\,(\boldsymbol{X}\boldsymbol{A}_i)\,, \quad i \in \{1, 2, 3, 4\}. \tag{38}$$

REMARK We recall that applicability of Lemma 1 requires both $\mathcal{P}_6$ and its dual to be solvable [17]. To this end, it suffices to show that there exists a pair $\{\hat{\boldsymbol{c}}_k, t\}$ that is strictly feasible for $\mathcal{P}_5$, with one example represented by $\{\hat{\boldsymbol{c}}_k, t\} = \{\boldsymbol{U}_{k-1}^\dagger \boldsymbol{d}_{0,k}, 1\}$. Then, strict feasibility of $\mathcal{P}_6$ (i.e., the corresponding SDR) is ensured via construction of the matrix

$$\begin{aligned} \boldsymbol{X}_F \triangleq\; & (1 - \xi)\, \boldsymbol{U}_c \left(\boldsymbol{e}_1 \boldsymbol{e}_1^\dagger \right) \boldsymbol{U}_c^\dagger \\ & + \frac{\xi}{L - k + 1} \boldsymbol{U}_c \left(\boldsymbol{I} - \boldsymbol{e}_1 \boldsymbol{e}_1^\dagger \right) \boldsymbol{U}_c^\dagger, \end{aligned} \tag{39}$$

where we have denoted $\boldsymbol{e}_1 \triangleq [\,1\;0\;\cdots\;0\,]^T$ and

$$\boldsymbol{U}_c \triangleq \begin{bmatrix} \boldsymbol{U}_F & \boldsymbol{0} \\ \boldsymbol{1}^T & 1 \end{bmatrix}, \tag{40}$$

which is built starting from the unitary matrix $\boldsymbol{U}_F \triangleq [\,\hat{\boldsymbol{c}}_k \;\; \boldsymbol{u}_1 \cdots \boldsymbol{u}_{L-k}\,]$. It can be easily verified that $\boldsymbol{X}_F \succ \boldsymbol{0}$ and also complies with the equality constraints in $\mathcal{P}_6$. Furthermore, the tunable parameter $\xi > 0$ in (39) can be made sufficiently small to satisfy the inequality constraint $\text{tr}\,(\boldsymbol{Q}_1 \boldsymbol{X}_F) > 0$. Differently, strict feasibility of the dual SDR, denoted here as $\mathcal{DP}_6$, can be easily verified from its direct inspection:

$$\mathcal{DP}_6 \triangleq \begin{cases} \min\limits_{y_1, y_2, y_3} & (y_2 + y_3) \\ \text{s.t.} & (-y_1 \boldsymbol{Q}_1 + y_2 \boldsymbol{Q}_2 + y_3 \boldsymbol{Q}_3 - \boldsymbol{Q}_0) \succeq \boldsymbol{0}\,, \\ & y_1 \geq 0. \end{cases} \tag{41}$$

It is apparent that proper combination (through y_2 and y_3) of $\boldsymbol{Q}_2$ and $\boldsymbol{Q}_3$ ensures positive definiteness and thus, strict feasibility. Finally, in Algorithm 1, we summarize the (sequential) procedure leading to an optimal solution to $\mathcal{P}_2$.

Algorithm 1
Algorithm to solve the radar waveform design problem $\mathcal{P}_2$.

Input: L, M, $\boldsymbol{S}$, $\boldsymbol{U}_{k-1}$, $\widehat{\boldsymbol{W}}$, $\boldsymbol{d}_{0,k}$, ϵ, γ;
Output: An optimal solution $\boldsymbol{c}_k^\star$ to problem $\mathcal{P}_2$;
1) solve problem $\mathcal{P}_6$, getting a solution $\boldsymbol{X}_{\text{sdr}}$;
2) find $\boldsymbol{x}^\star = \mathcal{D}(\boldsymbol{X}_{\text{sdr}}, \boldsymbol{Q}_0, \boldsymbol{Q}_1, \boldsymbol{Q}_2, \boldsymbol{Q}_3)$; let $\boldsymbol{x}^\star = [\,(\boldsymbol{z}^\star)^T \;\; y^\star\,]^T$;
3) set $\hat{\boldsymbol{c}}_k^\star = \boldsymbol{z}^\star / y^\star$.
4) return $\boldsymbol{c}_k^\star = \boldsymbol{U}_{k-1}\hat{\boldsymbol{c}}_k^\star$.

V. PERFORMANCE ANALYSIS

In the present section, we assess the reliability and the covertness of REM communication waveforms $\boldsymbol{c}_k^{\mathbf{Alg1}}$, for $k = 1, \dots K$, produced through Algorithm 1, in terms of SER and IM.

A. Simulation Setup

For our comparison we consider a unitary norm LFM pulse as the incident radar signal, with a duration $T = 133\ \mu$s, bandwidth $B = 750$ kHz, and a chirp rate $K_s = (\frac{750}{133} \times 10^9)$ Hz/s; when sampled at Nyquist rate f_s, we obtain the following discrete-time representation of $s(t)$:

$$s(n) = \frac{1}{\sqrt{N}} e^{j2\pi \frac{K_s}{2}((n-1)/f_s)^2}, \quad n = 1, \dots, N, \tag{42}$$

where $N = 100$. Differently, the signal is oversampled by the tag with a factor $M = 2$, thus resulting in additional DOFs. Clearly, an analogous discrete-time representation as (42) is obtained at the tag when substituting $f_s = MB$ and $N = 200$ samples. The number of communication waveforms (symbols) is set to $K = 4$ (2 bits). As explained in Section II, the ambient radar scatter $\boldsymbol{x}$ and noise $\boldsymbol{n}$ are modeled as $\boldsymbol{x} \sim \mathcal{CN}(\boldsymbol{0}, \frac{1}{MN}\boldsymbol{I})$ and $\boldsymbol{n} \sim \mathcal{CN}(\boldsymbol{0}, \frac{1}{MN}\boldsymbol{I})$, and the average power of the embedded communication signal, the ambient radar scatter (the interference), and the noise in (2) are each scaled to achieve the desired levels of SIR and SNR. Otherwise stated, given the received signal model $\boldsymbol{y}_{rk}$ of (2), we consider $\alpha_k = \sqrt{\text{SNR}}$ and $\beta = \sqrt{\text{SNR}/\text{SIR}}$. Furthermore, we set $L = 100$. Finally, with reference to the similarity constraint in (12), we set $\hat{N} = 8\,MN$ and $F = 4\,MN + 6 = 806$, respectively.

For completeness of comparison, we report the SER and the interception curves for the following four design techniques:

1) The eigenvectors-as-waveform (EAW) approach of [2], where the K eigenvectors corresponding to the K smallest eigenvalues are used as communication symbols, namely, $\boldsymbol{c}_k^{\text{EAW}} \triangleq \boldsymbol{v}_k$, $k = 1, \dots, K$, with $\boldsymbol{v}_1, \dots, \boldsymbol{v}_K$ being the eigenvectors associated with the K smallest eigenvalues.

2) The weighted-combining (WC) approach of [2], where the K symbols are drawn out properly weighting a set of L nondominant eigenvectors with different weight vectors $\boldsymbol{b}_k \in \mathbb{C}^{L\times 1}$, $k = 1, \dots, K$, known only to the tag and the intended receiver; namely, letting $\boldsymbol{V}_{\text{ND}} = [\boldsymbol{v}_1 \dots \boldsymbol{v}_L]$, $\boldsymbol{c}_k^{\text{WC}} \triangleq \boldsymbol{V}_{\text{ND}}\,\boldsymbol{b}_k$, $k = 1, \dots, K$. In what follows, we draw $\boldsymbol{b}_k \sim \mathcal{CN}(\boldsymbol{0}, \boldsymbol{I})$, and $\boldsymbol{c}_k^{\text{WC}}$ is scaled to have unitary norm.

3) The DP approach of [2], where the K waveforms are sequentially designed by projecting away from the (accumulated) whole dominant space a set of pseudorandom vectors $\boldsymbol{d}_k^{\text{DP}} \in \mathbb{C}^{MN\times 1}$, $k = 1, \dots, K$, available only at the tag and the intended receiver. Precisely, $\boldsymbol{c}_k^{\text{DP}} \triangleq \boldsymbol{P}_{k-1}\boldsymbol{d}_k^{\text{DP}}$, $k = 1, \dots, K$. In the following, $\boldsymbol{d}_k^{\text{DP}} \sim \mathcal{CN}(\boldsymbol{0}, \boldsymbol{I})$,and $\boldsymbol{c}_k^{\text{DP}}$ is scaled to have unitary norm.

4) The minimum LPI approach, where the K communication waveforms are devised so as to minimize the IM (14) for all the projection matrices $\tilde{\boldsymbol{P}}_\ell$, $\ell = 1, \dots, MN - 1$, namely, $\boldsymbol{c}_k^{\text{LPI}}$ is an optimal solution for the optimization problem [7]

$$\mathcal{P}_{\text{LPI}} \triangleq \begin{cases} \min\limits_{\boldsymbol{c}_k} & \boldsymbol{c}_k^\dagger \tilde{\boldsymbol{P}} \boldsymbol{c}_k \\ \text{s.t.} & \boldsymbol{P}_{k-1}^\perp \boldsymbol{c}_k = \boldsymbol{0}, \quad \boldsymbol{c}_k^\dagger \boldsymbol{c}_k = 1, \\ & \left\| \widehat{\boldsymbol{W}} \boldsymbol{c}_k - \widehat{\boldsymbol{W}} \boldsymbol{d}_{0,k} \right\|^2 \le \epsilon, \end{cases} \tag{43}$$

where the matrix $\tilde{\boldsymbol{P}}$, accounting for the weighted sum of the projection matrices, is defined as in $\mathcal{P}_2$.

As to the filtering strategy, following the hint of [2], we assume that the intended receiver may employ:

1) a MF, i.e., $\boldsymbol{w}_k = \boldsymbol{c}_k$, $k = 1, \dots, K$;
2) a DF,[8] i.e., $\boldsymbol{w}_k = (\boldsymbol{C}\boldsymbol{C}^\dagger)^{-1}\boldsymbol{c}_k$, $k = 1, \dots, K$, where $\boldsymbol{C} \triangleq [\boldsymbol{S}\,\boldsymbol{c}_1 \;\dots\; \boldsymbol{c}_K]$.

Given the received signal $\boldsymbol{y}_r$, at the receiver side an embedded communication symbol $\bar{\boldsymbol{c}}$ is extracted as

$$\bar{\boldsymbol{c}} \triangleq \arg \max_{\{\boldsymbol{c}_1, \boldsymbol{c}_2, \dots, \boldsymbol{c}_K\}} |\boldsymbol{w}_k^\dagger\, \boldsymbol{y}_r|. \tag{44}$$

Thus, for each of the aforementioned waveform design technique, the following experiments have been considered:

1) For what concerns the evaluation of the SER performance, firstly we design 10 sets of K communication symbols[9]; then, for each set, we consider 10^5 independent identically distributed (iid) realizations of the noise and the interference impairments, which results in 10^5 iid instances of the received signal $\boldsymbol{y}_{rk}$. Aiming at a fair comparison, we use the same disturbance set for all the K symbols. By doing so, we intend to test their effectiveness under the same impairment conditions. For each of the $K \times 10^5$ realizations of the received signal, we apply the decision rule (44) and declare a successful

[7] Clearly, also $\mathcal{P}_{\text{LPI}}$ can be solved optimally in an efficient way, similarly as for $\mathcal{P}_2$.

[8] In what follows, we do not report the performance for the filter that maximizes the SIR in (4), i.e., $\boldsymbol{w}_k = (\boldsymbol{S}\boldsymbol{S}^\dagger)^{-1}\boldsymbol{c}_k$. The reason is that nearly identical behavior to the DF has been observed numerically in the considered scenarios.

[9] Different sets of K symbols correspond to different instances for the random vectors $\boldsymbol{b}_k$, $\boldsymbol{d}_k{}^{\text{DP}}$, and $\boldsymbol{d}_k$, respectively for the WC, DP, and Algorithm 1 approaches. By iterating the experiment over a multitude of possible sets, we aim at reducing the variation of SER with respect to set selection.

transmission only when $\bar{\boldsymbol{c}}$ effectively equals the transmitted waveform (namely, the embedded communication symbol is correctly extracted). The SER performance is, hence, evaluated accordingly. Finally, the SER is averaged over the total number of available sets. The experiment is performed for three different values of SIR (i.e., SIR $\in \{-40, -35, -30\}$ dB), assuming an SNR $\in [-15, 0]$ dB.

2) For what concerns the evaluation of the IM (14), we first generate 10 different sets of K symbols[10]; then, for each set, we consider 200 iid realizations of the noise and the interference components, and assume that the waveform corresponding to the index $k = 1$ is transmitted by the tag.[11] This results in 200 realizations of the received signal $\boldsymbol{y}_{1r} = \alpha_1 \boldsymbol{c}_1 + \beta \boldsymbol{S}\boldsymbol{x} + \boldsymbol{n}$ for each of the 10 sets. The LPI behavior of the devised symbol is, therefore, estimated by ascertaining the IM through (14) and averaging it over the total number of disturbance realizations and the total number of available sets. The experiment is performed assuming SIR = –35 dB and SNR = –10 dB.

B. Simulation Results

In Figs. 2– 4, we analyze the SER versus SNR for the symbols $\boldsymbol{c}_k^{\mathbf{Alg1}}$, for different values of the similarity parameter ϵ and the Pareto weight γ (when either a MF or a DF is employed at the receiver side) and compare the results with those achieved by $\boldsymbol{c}_k{}^{\mathrm{LPI}}$ (in Figs. 2–4), $\boldsymbol{c}_k{}^{\mathrm{EAW}}$ (in Fig. 2), $\boldsymbol{c}_k{}^{\mathrm{WC}}$ (in Fig. 3), and $\boldsymbol{c}_k{}^{\mathrm{DP}}$ (in Fig. 4). More specifically, Fig. 2a 1, 2b 1, 2c 1, and 2d 1 refer to the MF, for $\epsilon = 0.01$, 0.05, 0.1, and 0.5, respectively. Conversely, Fig. 2a 2, 2b 2, 2c 2, and 2d 2 refer to the DF, for $\epsilon = 0.01$, 0.05, 0.1, and 0.5, respectively. The same structure has been adopted for the plots shown in Figs. 3 and 4. With reference to $\boldsymbol{c}_k{}^{\mathbf{Alg1}}$, we report the results for $\gamma = 0$, 2, and 2.3.

A first inspection of the curves obtained with $\boldsymbol{c}_k{}^{\mathbf{Alg1}}$ reveals that lower SER is achieved with small values of γ; such behavior is a direct consequence of the mediative role of the Pareto weight between the two actors involved in the optimization problem. In fact, the importance of the reliability of the embedded communication over its covertness grows considerably as γ is decreased (we recall that these features are represented, respectively, by the maximization of the first component and the minimization of the remaining components of the vectorial optimization function of $\mathcal{P}_1$); hence, we expect higher interception probabilities to be swapped for lower SER values. Indeed, in the extreme case $(\gamma, \epsilon) = (0, 2)$, we expect that SER performance will attain those of EAW. This can be explained because in the mentioned scenario the similarity

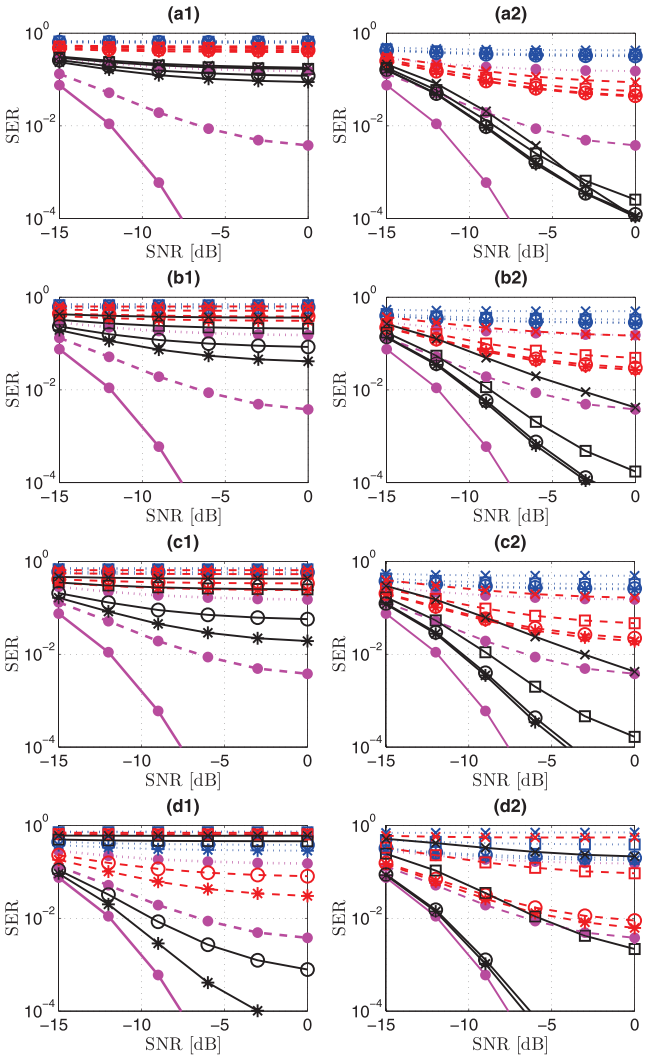

Fig. 2. Upper panel: (a1) $\varepsilon = 0.01$, MF; (a2) $\varepsilon = 0.01$, DF; (b1) $\varepsilon = 0.05$, MF; (b2) $\varepsilon = 0.05$, DF. Lower panel: (c1) $\varepsilon = 0.1$, MF; (c2) $\varepsilon = 0.1$, DF; (d1) $\varepsilon = 0.5$, MF; (d2) $\varepsilon = 0.5$, DF. SER versus SNR (dB); SIR = –30 dB (continuous lines); SIR = –35 dB (dashed lines); SIR = –40 dB (dotted lines). EAW: •-marked curves; Alg. 1, $\gamma = 0$: *-marked curves; Alg. 1, $\gamma = 2$: ○-marked curves; Alg. 1, $\gamma = 2.3$: □-marked curves; min. LPI: x-marked curves.

constraint is not active and $\gamma = 0$ implies sequential (output) SIR maximization, whose closed form solution is the EAW design itself.

This intuition is partially confirmed by a comparison of the results obtained for different similarity parameters. Indeed, the plots highlight the capability, of the proposed approach, to attain remarkable SER improvements (namely, to ensure more and more reliable communications) as ϵ increases, when $\gamma \in \{0,2\}$. Conversely, when higher values of γ are adopted (for instance, $\gamma = 2.3$), the symbols $\boldsymbol{c}_k{}^{\mathbf{Alg1}}$ experience a partial loss in terms of SER profiles (on behalf of more and more covert embedded transmissions), which becomes heavier as the similarity constraint is loosen. For instance, with reference to the MF, we can easily observe this effect by a comparison of Fig. 2a 1, 2b 1, 2c 1, and 2d 1; the same

[10] As for the SER evaluation, we iterate the experiment over a multitude of possible sets in order to reduce the variation of the IM (14) with respect to set selection.

[11] Indeed, it has been observed numerically that considering other waveforms in the set leads to similar behaviors in terms of intercept curves.

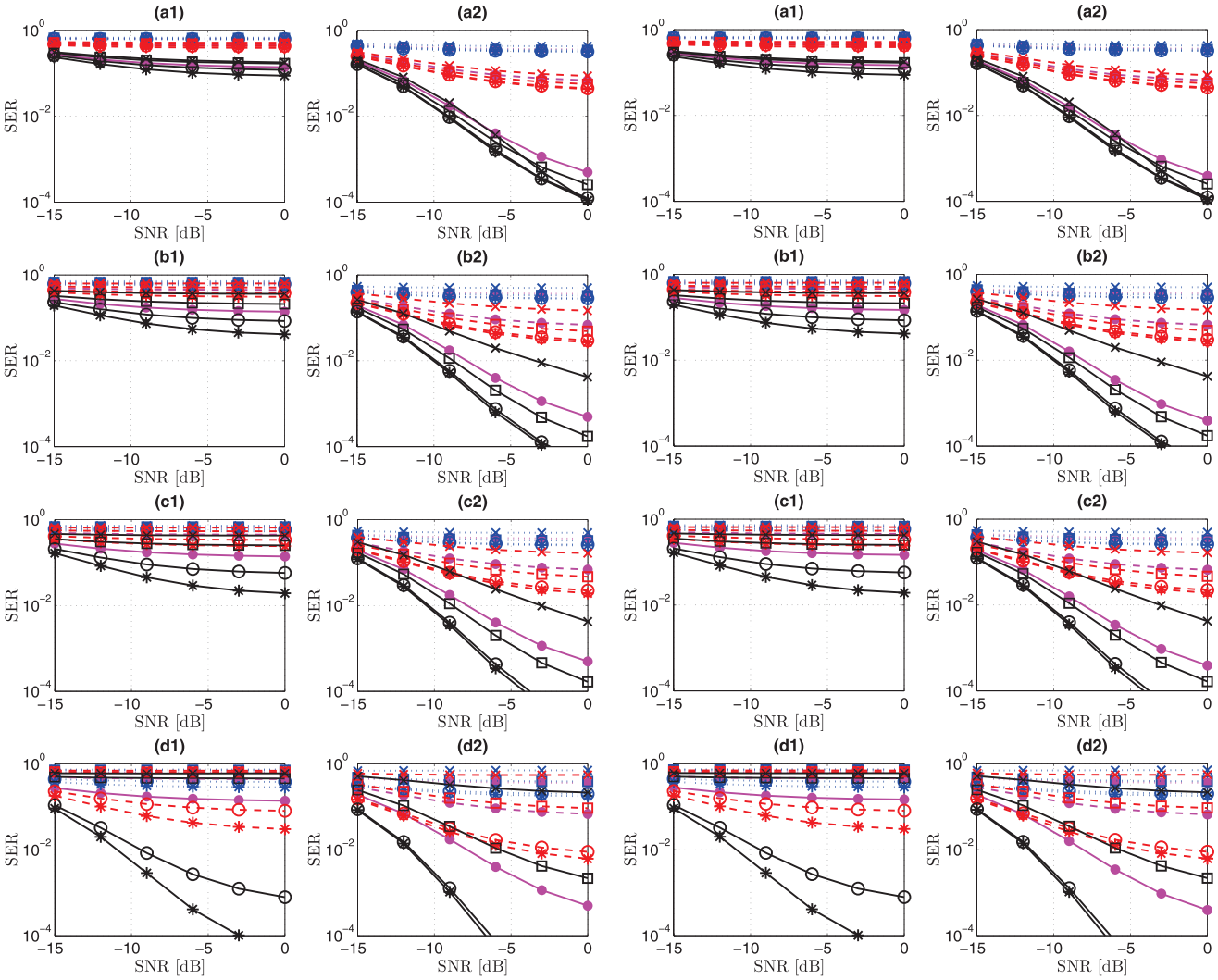

Fig. 3. Upper panel: (a1) $\epsilon = 0.01$, MF; (a2) $\epsilon = 0.01$, DF; (b1) $\epsilon = 0.05$, MF; (b2) $\epsilon = 0.05$, DF. Lower panel: (c1) $\epsilon = 0.1$, MF; (c2) $\epsilon = 0.1$, DF; (d1) $\epsilon = 0.5$, MF; (d2) $\epsilon = 0.5$, DF. SER versus SNR (dB); SIR = –30 dB (continuous lines); SIR = –35 dB (dashed lines); SIR = –40 dB (dotted lines). WC: •-marked curves; Alg. 1, $\gamma = 0$: *-marked curves; Alg. 1, $\gamma = 2$: ○-marked curves; Alg. 1, $\gamma = 2.3$: □-marked curves; min. LPI: x-marked curves.

Fig. 4. Upper panel: (a1) $\epsilon = 0.01$, MF; (a2) $\epsilon = 0.01$, DF; (b1) $\epsilon = 0.05$, MF; (b2) $\epsilon = 0.05$, DF. Lower panel: (c1) $\epsilon = 0.1$, MF; (c2) $\epsilon = 0.1$, DF; (d1) $\epsilon = 0.5$, MF; (d2) $\epsilon = 0.5$, DF. SER versus SNR (dB); SIR = –30 dB (continuous lines); SIR = –35 dB (dashed lines); SIR = –40 dB (dotted lines). DP: •-marked curves; Alg. 1, $\gamma = 0$: *-marked curves; Alg. 1, $\gamma = 2$: ○-marked curves; Alg. 1, $\gamma = 2.3$: □-marked curves; min. LPI: x-marked curves.

phenomenon occurs when a DF is employed (see Fig. 2a 2, 2b 2, 2c 2, and 2d 2). This is not surprising because relaxing the similarity constraint is tantamount to enlarging the feasible set: hence, additional DOFs are at disposal for the optimization procedure, which can be potentially exploited to further refine the most relevant components of the vectorial optimization function. Specifically, when the relative weight of the interception feature is more prominent (γ is large), we expect that the additional DOFs are spent to lower the interceptability of the transmission, of course to the detriment of its intelligibility. The inverse happens when the reliability characteristic assumes greater importance (γ is small): the error rates diminish because higher SIR values are attained, in response to the widening of the similarity set. On the other hand, when ϵ is taken to be very small, it is expected (as confirmed by simulations) that both $\boldsymbol{c}_k^{\mathbf{Alg1}}$ and $\boldsymbol{c}_k^{\mathrm{LPI}}$ design collapse to a DP design because the similarity constraint enforces a strict similarity to noise-like waveforms that are made weakly correlated and orthogonal to the dominant space (this is indeed the natural outcome of the constraint $\boldsymbol{P}_{k-1}^{\perp}\boldsymbol{c}_k = \boldsymbol{0}$, $k = 1, \ldots, K$). From the analysis, we can also ascertain the effectiveness of the interference cancellation capability of the DF over the MF for all the considered waveform designs because the former filtering strategy substantially outperforms the latter.

Furthermore, SER of EAW approach is identical with both MF and DF, and is lower than that achieved with Algorithm 1. Indeed the symbols $\boldsymbol{c}_k^{\mathrm{EAW}}$ exploit the eigenvectors possessing the least correlation with the ambient backscatter; hence, they are more easily pulled

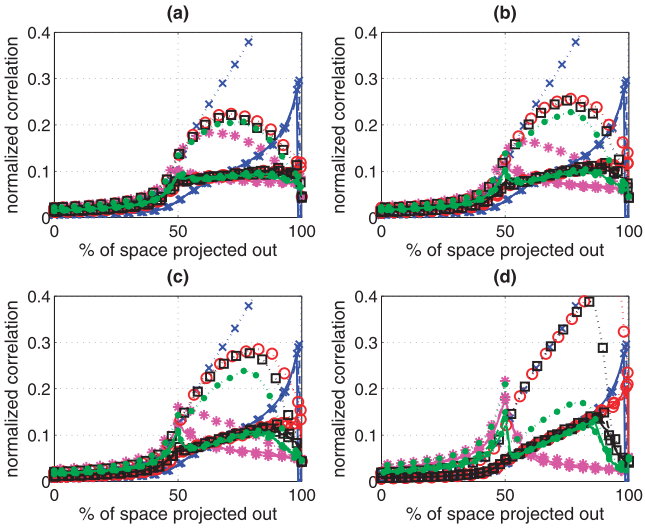

Fig. 5. Intercept metric. Waveform 1 (dotted lines); waveform 2 (dashed lines); waveform 3 (dot-dashed lines); waveform 4 (continuous lines). EAW: x-marked blue curves; Alg. 1, $\gamma = 0$: ○-marked red curves; Alg. 1, $\gamma = 2$: □-marked black curves; Alg. 1, $\gamma = 2.3$: •-marked green curves; min. LPI: *-marked magenta curves. (a) $\epsilon = 0.01$; (b) $\epsilon = 0.05$; (c) $\epsilon = 0.1$; (d) $\epsilon = 0.5$.

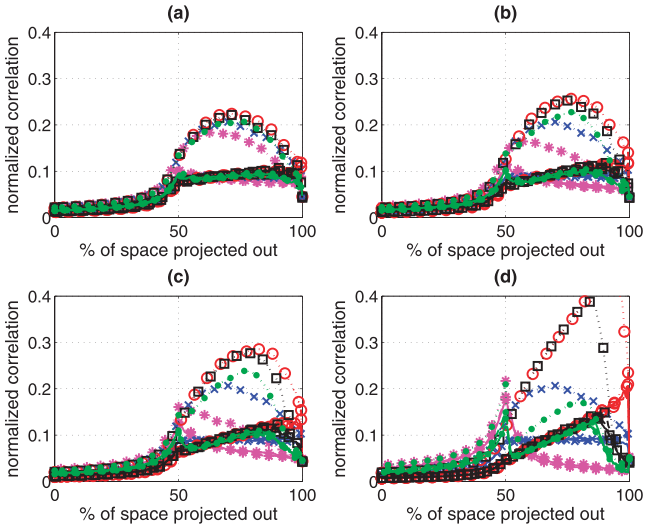

Fig. 6. Intercept metric. Waveform 1 (dotted lines); waveform 2 (dashed lines); waveform 3 (dot-dashed lines); waveform 4 (continuous lines). WC: x-marked blue curves; Alg. 1, $\gamma = 0$: ○-marked red curves; Alg. 1, $\gamma = 2$: □-marked black curves; Alg. 1, $\gamma = 2.3$: •-marked green curves; min. LPI: *-marked magenta curves. (a) $\epsilon = 0.01$; (b) $\epsilon = 0.05$; (c) $\epsilon = 0.1$; (d) $\epsilon = 0.5$.

out from the received signal than $\boldsymbol{c}_k{}^{\mathbf{Alg1}}$ (which are instead designed to exhibit a partial correlation with the ambient backscatter). Also, because each waveform $\boldsymbol{c}_k{}^{\mathrm{EAW}}$ is associated to a distinct eigenvector of $\boldsymbol{S}\boldsymbol{S}^{\dagger}$, EAW does not get any profit from the cancellation (prewhitening) capability provided by the DF (i.e., $\boldsymbol{c}_k{}^{\mathrm{EAW}}$ already provide interference suppression). On the other hand, when $\gamma \in \{0,2\}$, the proposed approach is comparable with, or totally outperforms, both WC and DP strategies in terms of reliability. This outcome can be easily explained noticing that, for the above values of γ, the SIR levels attained with the codes $\boldsymbol{c}_k{}^{\mathbf{Alg1}}$ are still higher than those achieved by $\boldsymbol{c}_k{}^{\mathrm{WC}}$ and $\boldsymbol{c}_k{}^{\mathrm{DP}}$. Therefore, even if all the three techniques possess a partial correlation with the ambient backscatter (in spite of EAW), the proposed waveform design strategy still allows for easier extraction of the embedded symbol for the intended receiver. When $\gamma = 2.3$, we experience a SER degradation with respect to EAW, WC, and DP approaches. As already highlighted, this loss is due to the existing trade-off between the SER profile and the covertness capability of the tag; we presume that this loss will be paid off with lower probabilities of interception. Finally, we observe that, when a MF is adopted, $\boldsymbol{c}_k{}^{\mathrm{LPI}}$ achieves similar SER to $\boldsymbol{c}_k{}^{\mathrm{Alg1}}$ for $\gamma = 2.3$; different situation occurs, instead, with the DF.

In Figs. 5–7, we show the IM of the symbols $\boldsymbol{c}_k{}^{\mathbf{Alg1}}$, for $\epsilon \in \{0.01, 0.05, 0.1, 0.5\}$ and $\gamma \in \{0, 2, 2.3\}$, and compare the results with those obtained by the codes $\boldsymbol{c}_k{}^{\mathrm{LPI}}$ (in Figs. 5–7), $\boldsymbol{c}_k{}^{\mathrm{EAW}}$ (in Fig. 5), $\boldsymbol{c}_k{}^{\mathrm{WC}}$ (in Fig. 6), and $\boldsymbol{c}_k{}^{\mathrm{DP}}$ (in Fig. 7). The trend of the proposed technique is in line with that displayed in the above analysis. Specifically, higher values of γ correspond to lower correlation values for waveform 1 obtained with Algorithm 1, and the IM of $\boldsymbol{c}^{\mathrm{LPI}}$ is approached in this case, which denotes the actual

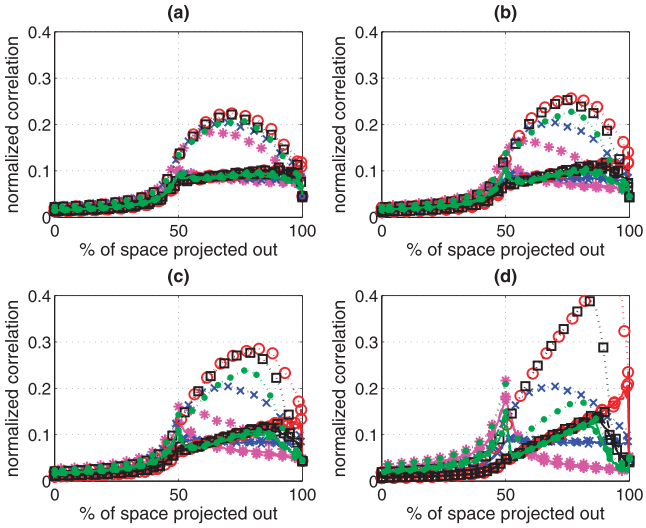

Fig. 7. Intercept metric. Waveform 1 (dotted lines); waveform 2 (dashed lines); waveform 3 (dot-dashed lines); waveform 4 (continuous lines). DP: x-marked blue curves; Alg. 1, $\gamma = 0$: ○-marked red curves; Alg. 1, $\gamma = 2$: □-marked black curves; Alg. 1, $\gamma = 2.3$: •-marked green curves; min. LPI: *-marked magenta curves. (a) $\epsilon = 0.01$; (b) $\epsilon = 0.05$; (c) $\epsilon = 0.1$; (d) $\epsilon = 0.5$.

lower bound for the considered figure of merit (cf. Fig. 5a). Hence, it is possible to prevent a hostile eavesdropper from extracting the embedded signal and from actually becoming aware of the transmission. From this point of view, our approach surpasses EAW, WC, and DP, substantially always ensuring lower correlation values when γ is sufficiently big. On the other hand, the covertness capabilities of the embedded communication worsen for smaller weights because the SIR component is advantaged in the optimization procedure (however, the

IM is quite low, thus a covert conversation is still virtually possible). Moreover, the correlation values for waveforms 2, 3, and 4 are smaller: this implies that an intended receiver, provided a previous knowledge of the related symbols, would be easily able to discern which is the symbol embedded in the actual received signal, resorting to a coherent filtering.

By relaxing the similarity constraint (viz. increasing ϵ), this trend becomes more evident (cf. Fig. 5a–5d). In particular, when $\gamma = 2.3$ the proposed procedure ensures a more covert transmission; differently, the reverse effect is displayed for $\gamma \in \{0, 2\}$, where slightly higher correlation values are obtained for all the waveforms. These results confirm our previous insight: worse SER profiles can be swapped for better intercept features by properly tuning the weight γ. Furthermore, by increasing the similarity parameter, more DOFs are obtained due to the enlargement of the feasible set, which are spent to emphasize, in the optimization problem, the property holding the greatest importance. As to the reference design technique, when γ is kept limited, Algorithm 1 basically outperforms EAW approach for all the settings of ϵ; however, it displays a behavior comparable to those of WC and DP only when the similarity constraint is sufficiently tight ($\epsilon < 0.1$, for the case at hand), once again displaying the conflicting nature of the two actors involved in our optimization problem.

Summarizing, our analysis has shown that, by properly adjusting both the similarity level and the Pareto weight, the proposed design strategy proves to be better than, or at least comparable with, the EAW, WC, and DP approaches in terms of covertness and reliability of a radar-embedded communication between the tag and the intended receiver. Equally important, the EAW, DP, WC, and minimum LPI approaches can be seen as special instances of $\boldsymbol{c}_k^{\mathbf{Alg1}}$ when γ and ϵ are set to extreme values, thus confirming the generality of the proposed waveform design framework.

C. Computational Complexity

Finally, we discuss here the computational complexity of the proposed approach and of the other considered alternatives. Firstly, we observe that the heavier (in terms of complexity) step for the design of the waveform set of both EAW and WC approaches is represented by the eigendecomposition of the correlation matrix $\boldsymbol{S}\boldsymbol{S}^{\dagger}$. Thus, their complexity is dominated by the term $\mathcal{O}((MN)^3)$.

Secondly, the complexity of the DP approach is dominated by the K eigendecompositions required to project each waveform onto the (updated) nondominant space. In other words, for the kth waveform, the eigendecomposition $\boldsymbol{S}_{P,k-1}\boldsymbol{S}_{P,k-1}^{\dagger} = \boldsymbol{V}_{P,k-1}\boldsymbol{\Lambda}_{P,k-1}\boldsymbol{V}_{P,k-1}^{\dagger}$ is evaluated, where $\boldsymbol{S}_{P,k-1} \triangleq [\,\boldsymbol{S}\ \boldsymbol{c}_1\ \cdots\ \boldsymbol{c}_{k-1}\,] \in \mathbb{C}^{MN\times(2MN+k-2)}$. Therefore, its overall complexity is dominated by the term $\mathcal{O}(K(MN)^3)$.

Thirdly, we remark that the proposed approach will first require similar (in terms of complexity) eigendecompositions as the DP approach. Thus, the complexity required for the preprocessing of each sequential step is given by $\mathcal{O}((MN)^3)$. Also, the kth sequential optimization has been proved to share a worst-case order computational complexity $\mathcal{O}((L-k+1)^{4.5}\log(1/\xi))$ (ξ being the desired accuracy for the solution of the SDR) [26]. Furthermore, a (lower) complexity $\mathcal{O}((L-k+1)^3)$ is required for application of the rank-one decomposition theorem [17]. Therefore, the computation of the entire waveform set requires a complexity of $\mathcal{O}(\sum_{k=1}^{K}(L-k+1)^{4.5}\log(1/\xi))$. Collecting all the terms provides:

$$\mathcal{O}\left(K(MN)^3 + \sum_{k=1}^{K}\left[(L-k+1)^{4.5}\log\left(\xi^{-1}\right)\right]\right). \quad (45)$$

VI. CONCLUSIONS

In the present paper, we have focused on intrapulse REM communication where the incident radar illumination is remodulated, through an RF tag/transponder, into one of K information symbols. First, we have exploited the radar backscatter so that the devised symbols would possess a certain correlation with the ambient electromagnetic environment, which ensures a certain stealthiness level to the transmission. Then, we have devised our communication waveforms in accordance to the following criterion: jointly constrained optimization of both the reliability of the transmission (through the maximization of the SIR) and the covertness of the communication (through the minimization of an IM). The problem has been formulated in terms of a nonconvex multiobjective optimization problem with two quadratic constraints. Hence, tag symbols have been constructed as Pareto-optimal points of the aforementioned problem through the scalarization procedure. At the analysis stage, we have evaluated the performance of the new algorithm in terms of SER and LPI performance. The results have shown the capability of the proposed approach to suitably trade off the reliability and the covertness features of the established communication.

Possible future research tracks might concern the extension of the framework to situations where it is also necessary to account for the multipath effects and/or where it is necessary to force additional constraints on the structure of the radar waveform. Additionally, design of transmit-receive filters that account for the discovery of a tag transmission (as in [3]) and for possible timing uncertainties at the receiver will be object of future studies.

APPENDIX

Let us assume that $[\,(\boldsymbol{z}^{\star})^T\ y^{\star}\,]^T$ is optimal to $\mathcal{P}_5$; then, it follows that $\boldsymbol{c}^{\star} = \boldsymbol{z}^{\star}/y^{\star}$ is feasible to $\mathcal{P}_4$ because:

$$\begin{aligned}
&\operatorname{tr}\left(\boldsymbol{Q}_1\begin{bmatrix}\boldsymbol{z}^\star\\ y^\star\end{bmatrix}\begin{bmatrix}(\boldsymbol{z}^\star)^\dagger & (y^\star)^*\end{bmatrix}\right)\geq 0\\
&\Leftrightarrow \operatorname{tr}\left(\begin{bmatrix}-\boldsymbol{U}_{k-1}^\dagger\hat{\boldsymbol{W}}^\dagger\hat{\boldsymbol{W}}\boldsymbol{U}_{k-1} & \boldsymbol{U}_{k-1}^\dagger\hat{\boldsymbol{W}}^\dagger\hat{\boldsymbol{W}}\boldsymbol{d}_{0,k}\\ \left(\boldsymbol{U}_{k-1}^\dagger\hat{\boldsymbol{W}}^\dagger\hat{\boldsymbol{W}}\boldsymbol{d}_{0,k}\right)^\dagger & \epsilon-\boldsymbol{d}_{0,k}^\dagger\hat{\boldsymbol{W}}^\dagger\hat{\boldsymbol{W}}\boldsymbol{d}_{0,k}\end{bmatrix}\begin{bmatrix}\boldsymbol{z}^\star(\boldsymbol{z}^\star)^\dagger & (y^\star)^*\boldsymbol{z}^\star\\ y^\star(\boldsymbol{z}^\star)^\dagger & |y^\star|^2\end{bmatrix}\right)\geq 0 \qquad ;\\
&\Leftrightarrow (\boldsymbol{z}^\star)^\dagger(-\boldsymbol{U}_{k-1}^\dagger\hat{\boldsymbol{W}}^\dagger\hat{\boldsymbol{W}}\boldsymbol{U}_{k-1})\boldsymbol{z}^\star+2\Re\left\{(y^\star\boldsymbol{U}_{k-1}^\dagger\hat{\boldsymbol{W}}^\dagger\hat{\boldsymbol{W}}\boldsymbol{d}_{0,k})^\dagger\boldsymbol{z}^\star\right\}+|y^\star|^2(\epsilon-\boldsymbol{d}_{0,k}^\dagger\hat{\boldsymbol{W}}^\dagger\hat{\boldsymbol{W}}\boldsymbol{d}_{0,k})\geq 0\\
&\Leftrightarrow (c^\star)^\dagger(-\boldsymbol{U}_{k-1}^\dagger\hat{\boldsymbol{W}}^\dagger\hat{\boldsymbol{W}}\boldsymbol{U}_{k-1})\boldsymbol{c}^\star+2\Re\left\{(\boldsymbol{U}_{k-1}^\dagger\hat{\boldsymbol{W}}^\dagger\hat{\boldsymbol{W}}\boldsymbol{d}_{0,k})^\dagger c^\star\right\}+(\epsilon-\boldsymbol{d}_{0,k}^\dagger\hat{\boldsymbol{W}}^\dagger\hat{\boldsymbol{W}}\boldsymbol{d}_{0,k})\geq 0
\end{aligned}\tag{46}$$

$$\begin{aligned}
&\operatorname{tr}\left(\boldsymbol{Q}_2\begin{bmatrix}\boldsymbol{z}^\star\\ y^\star\end{bmatrix}\begin{bmatrix}(\boldsymbol{z}^\star)^\dagger & (y^\star)^*\end{bmatrix}\right)=1\Leftrightarrow\operatorname{tr}\left(\begin{bmatrix}\boldsymbol{I} & \boldsymbol{0}\\ \boldsymbol{0} & 0\end{bmatrix}\begin{bmatrix}\boldsymbol{z}^\star(\boldsymbol{z}^\star)^\dagger & (y^\star)^*\boldsymbol{z}^\star\\ y^\star(\boldsymbol{z}^\star)^\dagger & |y^\star|^2\end{bmatrix}\right)=1\\
&\Leftrightarrow\operatorname{tr}\left((\boldsymbol{z}^\star)^\dagger\boldsymbol{z}^\star\right)=1=|y^\star|^2\Leftrightarrow(\boldsymbol{c}^\star)^\dagger\boldsymbol{c}^\star=1.
\end{aligned}\tag{47}$$

$$\operatorname{tr}\left(\boldsymbol{Q}_3\begin{bmatrix}\boldsymbol{z}^\star\\ y^\star\end{bmatrix}\begin{bmatrix}(\boldsymbol{z}^\star)^\dagger & (y^\star)^*\end{bmatrix}\right)=1\Leftrightarrow\operatorname{tr}\left(\begin{bmatrix}\boldsymbol{0} & \boldsymbol{0}\\ \boldsymbol{0} & 1\end{bmatrix}\begin{bmatrix}\boldsymbol{z}^\star(\boldsymbol{z}^\star)^\dagger & (y^\star)^*\boldsymbol{z}^\star\\ y^\star(\boldsymbol{z}^\star)^\dagger & |y^\star|^2\end{bmatrix}\right)=1\Leftrightarrow|y^\star|^2=1;\tag{48}$$

Therefore, $v(\mathcal{P}_5)\leq v(\mathcal{P}_4)$. Conversely, if $\boldsymbol{c}^\star$ is the optimal to $\mathcal{P}_4$, it can be shown that $[(\boldsymbol{c}^\star)^T\ 1]^T$ is feasible to $\mathcal{P}_5$. Indeed:

$$(\boldsymbol{c}^\star)^\dagger\boldsymbol{c}^\star=1\Leftrightarrow\operatorname{tr}\left(\begin{bmatrix}\boldsymbol{I} & \boldsymbol{0}\\ \boldsymbol{0} & 0\end{bmatrix}\begin{bmatrix}\boldsymbol{c}^\star\\ 1\end{bmatrix}\begin{bmatrix}(\boldsymbol{c}^\star)^\dagger & 1\end{bmatrix}\right)=1;\tag{49}$$

$$\operatorname{tr}\left(\begin{bmatrix}\boldsymbol{0} & \boldsymbol{0}\\ \boldsymbol{0} & 1\end{bmatrix}\begin{bmatrix}\boldsymbol{c}^\star\\ 1\end{bmatrix}\begin{bmatrix}(\boldsymbol{c}^\star)^\dagger & 1\end{bmatrix}\right)=1;\tag{50}$$

$$\begin{aligned}
&(\boldsymbol{c}^\star)^\dagger(-\boldsymbol{U}_{k-1}^\dagger\widehat{\boldsymbol{W}}^\dagger\widehat{\boldsymbol{W}}\boldsymbol{U}_{k-1})\boldsymbol{c}^\star+2\Re\left\{(\boldsymbol{U}_{k-1}^\dagger\widehat{\boldsymbol{W}}^\dagger\widehat{\boldsymbol{W}}\boldsymbol{d}_{0,k})^\dagger\boldsymbol{c}^\star\right\}+(\epsilon-\boldsymbol{d}_{0,k}^\dagger\widehat{\boldsymbol{W}}^\dagger\widehat{\boldsymbol{W}}\boldsymbol{d}_{0,k})\geq 0\\
&\Leftrightarrow\operatorname{tr}\left(\begin{bmatrix}-\boldsymbol{U}_{k-1}^\dagger\widehat{\boldsymbol{W}}^\dagger\widehat{\boldsymbol{W}}\boldsymbol{U}_{k-1} & \boldsymbol{U}_{k-1}^\dagger\widehat{\boldsymbol{W}}^\dagger\widehat{\boldsymbol{W}}\boldsymbol{d}_{0,k}\\ \left(\boldsymbol{U}_{k-1}^\dagger\widehat{\boldsymbol{W}}^\dagger\widehat{\boldsymbol{W}}\boldsymbol{d}_{0,k}\right)^\dagger & \epsilon-\boldsymbol{d}_{0,k}^\dagger\widehat{\boldsymbol{W}}^\dagger\widehat{\boldsymbol{W}}\boldsymbol{d}_{0,k}\end{bmatrix}\begin{bmatrix}\boldsymbol{c}^\star(\boldsymbol{c}^\star)^\dagger & \boldsymbol{c}^\star\\ (\boldsymbol{c}^\star)^\dagger & 1\end{bmatrix}\right)\geq 0.
\end{aligned}\tag{51}$$

Hence, $v(\mathcal{P}_4)\leq v(\mathcal{P}_5)$. Therefore, we can conclude that $v(\mathcal{P}_4)=v(\mathcal{P}_5)$.

REFERENCES

[1] Ciuonzo, D., De Maio, A., Foglia, G., and Piezzo, M. Pareto-theory for enabling covert intrapulse radar-embedded communications. Presented at the *Proceedings of IEEE International Radar Conference*, Arlington, VA, May 2015.

[2] Blunt, S. D., Yatham, P., and Stiles, J. Intrapulse radar-embedded communications. *IEEE Transactions on Aerospace and Electronic Systems*, **46**, 3 (Jul. 2010), 1185–1200.

[3] Blunt, S. D., Metcalf, J. G., Biggs, C. R., and Perrins, E. Performance characteristics and metrics for intra-pulse radar-embedded communication. *IEEE Journal on Selected Areas in Communications*, **29**, 10 (Dec. 2011), 2057–2066.

[4] Hijaz, Z., and Frost, V. S. Exploiting OFDM systems for covert communication. In *IEEE Military Communications Conference (MILCOM)*, 2010, 2149–2155.

[5] Hounam, D., and Wagel, K.-H. A technique for the identification and localization of SAR targets using encoding transponders. *IEEE Transactions on Geoscience and Remote Sensing*, **39**, 1 (Jan. 2001), 3–7.

[6] Onoe, M., Hasebe, N., and Zamas, T. Radar reflectors with controllable reflection. *Electronics and Communications in Japan (Part I: Communications)*, **63**, 3 (1980), 51–58.

[7] Cantrell, B. H., Coleman, J. O., and Trunk, G. V. Radar communications. Naval Research Lab Report, Tech. Rep. 8515, 1981.

[8] Dobkin, D. M. *The RF in RFID: Passive UHF RFID in Practice*. Newnes, Oxford UK: Elsevier Science, 2007.

[9] Stockman, H. Communication by means of reflected power. *Proceedings of the IRE*, **36**, 10 (Oct. 1948), 1196–1204.

[10] Richardson, D. L., Stratmoen, S. A., Bendor, G. A., Lee, H. E., and Decker, M. J. Tag communication protocol & system. U.S. Patent 6329944, Dec. 2001.

[11] Axline, R. M., Sloan, G. R., and Spalding, R. E. Radar transponder apparatus and signal processing technique. U.S. Patent 5486830, Jan. 1996.

[12] Erricolo, D., Griffiths, H., Teng, L., Wicks, M. C., and Monte, L. L.
On the spectrum sharing between radar and communication systems.
In *2014 International Conference on Electromagnetics in Advanced Applications (ICEAA)*, Aug. 2014, 890–893.

[13] Bliss, D. W.
Cooperative radar and communications signaling: The estimation and information theory odd couple.
In *IEEE Radar Conference*, May 2014, 50–55.

[14] Boyd, S., and Vandenberghe, L.
Convex Optimization. New York, NY: Cambridge University Press, 2004.

[15] Sen, S., Tang, G., and Nehorai, A.
Multiobjective optimization of OFDM radar waveform for target detection.
IEEE Transactions on Signal Processing, **59**, 2 (Feb. 2011), 639–652.

[16] De Maio, A., Piezzo, M., Farina, A., and Wicks, M.
Pareto-optimal radar waveform design.
IET, Radar, Sonar & Navigation, **5**, 4 (Apr. 2011), 473–482.

[17] Ai, W., Huang, Y., and Zhang, S.
New results on Hermitian matrix rank-one decomposition.
Mathematical Programming, **128**, 1–2 (2011), 253–283.

[18] De Maio, A., Huang, Y., Palomar, D. P., Zhang, S., and Farina, A.
Fractional QCQP with applications in ML steering direction estimation for radar detection.
IEEE Transactions on Signal Processing, **59**, 1 (Jan. 2011), 172–185.

[19] Capon, J.
High-resolution frequency-wavenumber spectrum analysis.
Proceedings of the IEEE, **57**, 8 (Aug. 1969), 1408–1418.

[20] Li, J., Guerci, J. R., and Xu, L.
Signal waveform's optimal under restriction design for active sensing.
In *4th IEEE Workshop on Sensor Array and Multichannel Processing*, 2006, 382–386.

[21] Kay, S. M.
Fundamentals of Statistical Signal Processing, Detection Theory, Vol. 2. Upper Saddle River, NJ USA: Prentice Hall PTR, 1998.

[22] Picinbono, B.
On deflection as a performance criterion in detection.
IEEE Transactions on Aerospace and Electronic Systems, **31**, 3 (1995), 1072–1081.

[23] De Maio, A., Piezzo, M., Farina, A., and Wicks, M.
Pareto-optimal radar waveform design.
Presented at the *International Waveform Diversity and Design Conference (WDD)*, 2010.

[24] De Maio, A., Piezzo, M., Iommelli, S., and Farina, A.
Design of Pareto-optimal radar receive filter.
International Journal of Electronics and Telecommunications, **57**, 4 (2011), 477–481.

[25] Ben-Tal, A., and Nemirovski, A. S.
Lectures on Modern Convex Optimization: Analysis, Algorithms, and Engineering Applications. Philadelphia, PA: Society for Industrial and Applied Mathematics, 2001.

[26] Palomar, D. P., and Eldar, Y. C.
Convex Optimization in Signal Processing and Communications. Cambridge, England UK: Cambridge University Press, 2010.

Domenico Ciuonzo (S'11-M'14) received the B.Sc. and M.Sc. (summa cum laude) degrees in computer engineering and the Ph.D., respectively, in 2007, 2009, and 2013, from Second University of Naples (SUN), Aversa, Italy. Since 2014, he has been a postdoctoral researcher at DIETI, University of Naples, Federico II, Italy. His research interests are mainly in the areas of data fusion, statistical signal processing, target tracking and wireless sensor networks. His reviewing activity was recognized by IEEE Communications Letters and IEEE Transactions on Communications, which nominated him Exemplary Reviewer in 2013 and 2014, respectively. Currently, he serves as associate editor for the IEEE Aerospace and Electronic Systems.

Antonio De Maio was born in Sorrento, Italy, on June 20, 1974. He received the Dr.Eng. degree (with honors) and the Ph.D. degree in information engineering, both from the University of Naples Federico II, Naples, Italy, in 1998 and 2002, respectively. From October to December 2004, he was a visiting researcher with the U.S. Air Force Research Laboratory, Rome, NY. Currently, he is a full professor with the University of Naples Federico II. His research interest lies in the field of statistical signal processing with an emphasis on radar detection, optimization theory applied to radar signal processing, and multiple-access communications. Dr. De Maio is the recipient of the 2010 IEEE Fred Nathanson Memorial Award as the young (less than 40 years of age) AESS Radar Engineer 2010 whose performance is particularly noteworthy as evidenced by contributions to the radar art over a period of several years, with the following citation for: robust CFAR detection, knowledge-based radar signal processing, and waveform design and diversity.

Goffredo Foglia was born in Italy in 1977. He received the Dr.Eng. degree in telecommunication engineering in June 2003 from the University of Naples Federico II, Italy, and the Ph.D. in radar theory and techniques in February 2007 from the University of Cassino. In February 2004, he joined Elettronica S.p.A., Rome, Italy. He is author of more than 30 papers in international journals and conferences. His research interest lies in the field of radar signal processing and electronic support measure algorithms, systems, and jamming techniques.

Marco Piezzo received the Dr.Eng. degree (summa cum laude) in telecommunication engineering, and the Ph.D. degree in information engineering, both from the University of Naples Federico II, Italy, in 2009 and 2013, respectively. His research interest lie in optimization theory with an emphasis on radar signal processing. Currently, he is working at Elettronica S.p.A.